The SAXS Guide

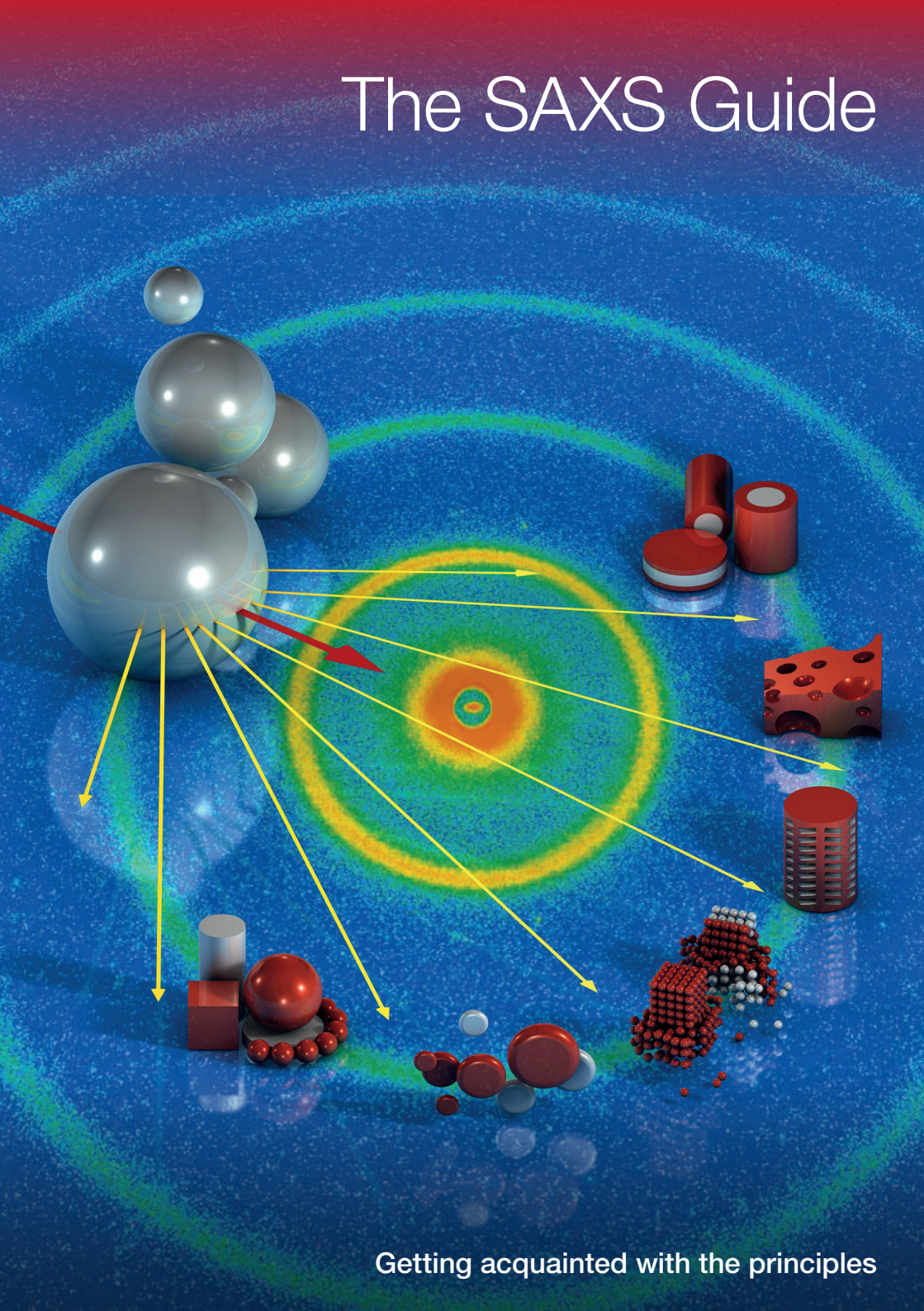

Getting acquainted with the principles

The SAXS Guide

Getting acquainted with
the principles

3rd edition

by
Heimo Schnablegger
Yashveer Singh

➤ Published by Anton Paar GmbH. Printed in Austria.

Anton Paar GmbH
Anton-Paar-Str. 20
A-8054 Graz
Austria - Europe
Tel.: +43 316 257-0
Fax: +43 316 257-257
E-Mail: info@anton-paar.com
Web: www.anton-paar.com

Date: June 2013

Specifications subject to change without notice. | 06/13 XPAIP019EN-C

Contents

1. Introduction

This document gives a general introduction to Small-Angle X-ray Scattering (SAXS) and SAXS analysis. It explains how a SAXS instrument works and how SAXS analysis is done. It is intended to help people new to the field of SAXS analysis. Difficult mathematical equations are avoided and the document requires only basic knowledge of mathematics, physics and colloid chemistry. The advanced reader is also encouraged to look for details in the original literature,[1]-[6] which can be found in the references section (see „Literature“ on page 112).

This document is not dedicated to one specific scattering instrument or one particular application area, but aims to give a global overview of the main instrumentation and applications.

2. What is SAXS

SAXS is an analytical method to determine the structure of particle systems in terms of averaged particle sizes or shapes. The materials can be solid or liquid and they can contain solid, liquid or gaseous domains (so-called particles) of the same or another material in any combination. Normally, X-rays are sent through the sample (transmission mode) and every particle that happens to be inside the beam will send out its signal. Thus, the average structure of all illuminated particles in the bulk material is measured.

But also surface-near particles can be measured selectively, when the X-rays hit a flat sample almost parallel to its surface and the scattering signal is measured in reflection mode. This relatively new variant of SAXS is called GI-SAXS (GI = grazing incidence) and it measures the average structure of all illuminated particles and their relative positional order on the surface or within the surface layer.

The SAXS method is accurate, non-destructive and usually requires only a minimum of sample preparation. Application areas are very broad and include biological materials, polymers, colloids, chemicals, nanocomposites, metals, minerals, food and pharmaceuticals and can be found in research as well as in quality control.

The samples that can be analyzed and the time requirements of the experiments mainly depend on the used instrumentation, which can be classified into two main groups, (1) the line collimation instruments and (2) the point collimation instruments, which are explained in more detail later. The particle or structure sizes that can be resolved range from 1 to 100 nm in a typical set-up but can be extended on both sides by measuring at smaller (Ultra Small-Angle X-Ray Scattering, USAXS) or larger angles (Wide-Angle X-Ray Scattering, WAXS also called X-Ray Diffraction, XRD) than the typical 0.1° to 10° of SAXS. The concentration ranges between 0.1 wt.% and 99.9 wt.%. Generally speaking, particles made of materials with high atomic numbers show higher contrast and have lower detection limits, when measured in matrix materials of lighter

elements. Matrix materials of heavy elements should be avoided due to their high absorption of X-rays.

Standards are required only in the following two situations:

1. When the **sample-to-detector distance** is not known. Then a reference sample of known structure is measured in order to calibrate the scattering angles. This is required only for instruments that employ unreliable mechanical movements and have poorly documented detector or sample positions.

2. When the **number density** of particles or their **mean molecular weight** has to be determined. Then the experimental intensities must be scaled by the intensity from a standard sample, such as water. For the determination of the particle structure, however, this is not required at all.

Fig. 2 - 1 shows a typical pair of scattering profiles of a dispersion of particles and of the solvent alone. The difference between these two profiles is the actual signal and is put into calculations in order to obtain the information of size, shape, inner structure or the specific surface of the particles.

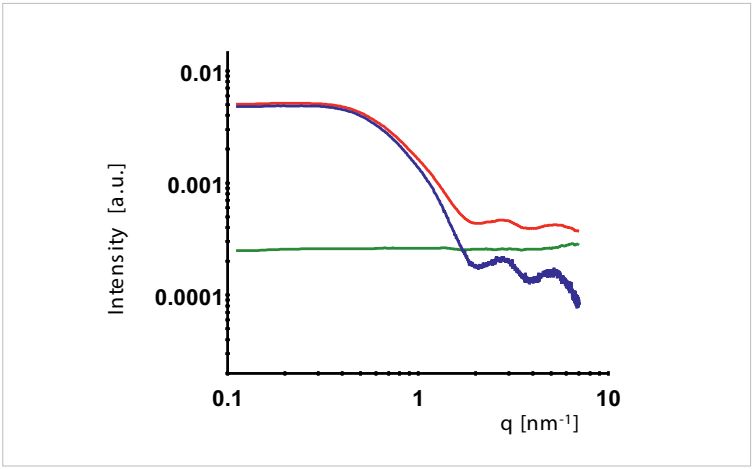

Fig. 2 - 1.

Typical SAXS profiles of (red) a particle dispersion, (green) of the solvent and (blue) the difference profile therefrom

➤ 2.1. Scattering and microscopy

Scattering and absorption are the first processes in any technique that uses radiation, such as an optical microscope (see Fig. 2 - 2.). This means that interaction between matter and the incoming radiation must take place. Otherwise no picture of the investigated object (= particle) will be available. Neither with microscopy nor with scattering can an object be investigated, when there is no contrast. In order to establish contrast in SAXS, the particles must have an electron density different than that of the surrounding matrix material (e.g., the solvent).

Although the operation of a scattering instrument is identical to the first process that takes place in a microscope, its result is complementary to that of a microscope, as will be outlined below.

The second process in an optical microscope is the reconstruction of the object (particle) from the scattering pattern (see Fig. 2 - 2.). This is done with the help of a lens system. If a lens system is not readily available for the used radiation (such as X-rays), then a reconstruction is not directly possible. Instead, the scattering pattern must be recorded and the reconstruction must be attempted in a mathematical way rather than in an optical way.

In the recording process the phases of the detected waves are lost. This constitutes the main difference between microscopy and X-ray scattering. Because of the lost phases, it is not possible to achieve a 3D (holographic) representation of the object in a direct way, as it would be possible with a lens system.

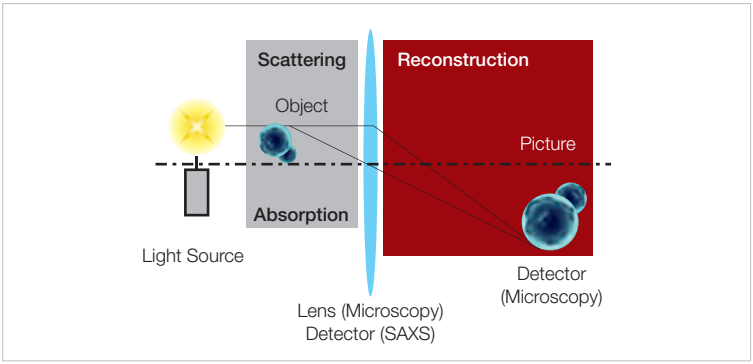

Fig. 2 - 2.

The first processes of a microscopic investigation are scattering and absorption. Microscopy: The scattered waves are processed into a picture (reconstructed) by a lens. SAXS: The scattered intensity is recorded by a detector and is processed mathematically, as a replacement for the actions of a lens.

In microscopy one object or a small part of a sample is magnified and investigated. With scattering techniques the whole illuminated sample volume is investigated. As a consequence, average values of the structure parameters are obtained by SAXS. The average is taken over all objects and over all orientations of the objects. Therefore, structure details of the object will not become visible unless they are pronounced enough in the whole sample and are therefore representative.

The signal strength in SAXS scales with the squared volume of the particle. This means that small particles are hardly visible in the presence of big particles. On the other hand, SAXS is very sensitive to the formation or growth of large particles.
The resolution criteria in SAXS are the same as those in microscopy. The closer the lens to the object (the larger the aperture or the scattering angle), the smaller is the detail that can be resolved. The farther away the object is from the lens (the smaller the aperture or the scattering angle), the bigger is the largest object that can be brought into the picture.

The following table summarizes a typical comparison of the two techniques.

Feature	Microscopy	Scattering
Small details are	visible	not visible
Results are	unique but not representative	representative but ambiguous
Local structure details	can be extracted	cannot be extracted
Average structures are	hard to obtain	always obtained
Preparation artifacts are	inherent	scarce (in vitro experiments)

In order to get the complete picture of an unknown sample one needs to make use of both methods, because **their results are complementary.**

3. Basics of SAXS

When X-rays irradiate a sample, then

1. the atoms inside the sample will scatter the incident radiation into all directions, which gives a background radiation that is almost constant at small angles.

2. the particles (i.e., clusters of atoms) inside the sample will produce additional scattering (so-called excess scattering) which is due to the fact that the particles are made of a different material or density (to give contrast) and are in the size-range of the X-ray wavelength.

By measuring the angle-dependent distribution of the scattered radiation (intensity) it is possible to draw conclusions about the average particle structure.

➤ 3.1. What are X-rays

X-rays are electro-magnetic waves just like “ordinary” visible light. But the wavelength is much shorter (<0.3 nm) than that of visible light (~500 nm). The waves propagate, because an alternating electric field ($\vec{E}$) causes an alternating magnetic field ($\vec{H}$) and vice versa (see Fig. 3 - 3.). The electric field, the magnetic field and the direction of propagation are always at right angles with respect to each other.

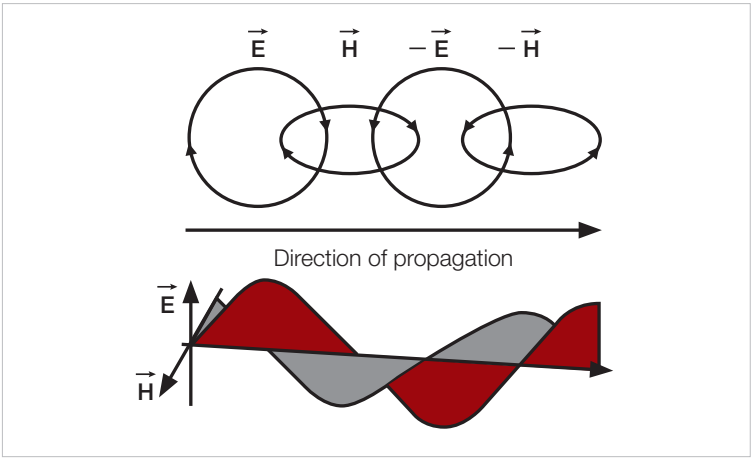

Fig. 3 - 3.

Electro-magnetic waves propagate due to induction processes. Close to the light source, the electric and the magnetic fields are phase shifted as shown here. Far away from the source, however, the two fields oscillate in phase.

Sometimes X-rays are described by particles called photons. Therefore, every interaction between light and matter can be described by two models, the oscillator model (wave) and the impulse-transfer model (photon).

➤ 3.2. Interaction of X-rays with matter

There are two main interactions of X-rays with matter: absorption and scattering. If X-rays hit a material, a fraction will pass through the sample, a fraction will be absorbed and transformed into other forms of energy (heat, fluorescence radiation, etc.) and a fraction will be scattered into other directions of propagation.

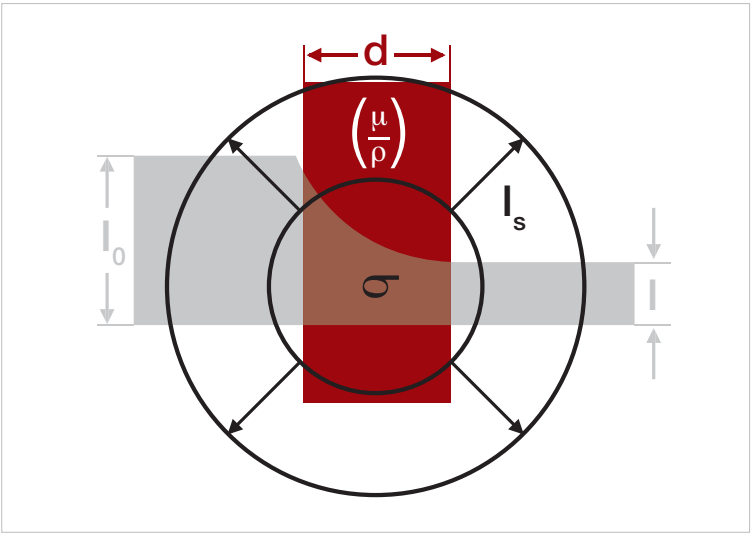

Fig. 3 - 4.

Incoming X-rays of intensity I_0 are attenuated to an intensity I and partly converted into scattered X-rays of intensity I_s by a material of thickness d, density (ρ), mass-absorption coefficient $\left(\frac{\mu}{\rho}\right)$ and scattering cross-section (σ).

3.2.1 Absorption

Irradiation of an atom with X-ray photons can expel an electron from the atom. By doing so the X-ray energy is used up and the photon is absorbed. This leaves the atom in an unstable situation with a hole, where there was an electron before. The atom wants to restore the original configuration, and this is done by rearranging the remaining electrons in order to fill up the hole. As a result of this, the atom emits fluorescence radiation, i.e., X-rays with other wavelengths than the incident radiation.

The absorption of an X-ray photon is most efficient at the so-called absorption edges, where the electrons of the material have the highest probability to be expelled. Absorption basically occurs at all wavelengths with various efficiencies. Depending on the atomic species of the material and on the wavelength, these absorption efficiencies are tabulated[7] as so-called mass-absorption

coefficients $(\frac{\mu}{\rho})$, where μ is the linear absorption coefficient and ρ is the density of the material.
In order to obtain high-quality SAXS data the absorption must be kept small. The optimum sample thickness d_{opt} depends on the linear absorption coefficient,

$$d_{opt} = \frac{1}{\mu}, \qquad [cm]$$

Typical values for d_{opt} at commonly used wavelengths are summarized in Table 3.1:.

Table 3.1:
The optimum sample thickness d_{opt} in [µm] of various matrix materials at commonly used X-ray wavelengths.

Radiation Wavelength	Cr-Ka 0.2291 nm	Cu-Ka 0.1542 nm	Mo-Ka 0.07107 nm	Density [g/mL]
water, 4°C	301.6	980.8	9886	1.0
quartz glass	41.0	126.6	1351	2.203
chloroform, 15°C	23.9	70.5	718	1.498
iron metal	11.4	4.22	36.8	7.86
tungsten metal	1.15	3.08	5.70	19.3

3.2.2 Scattering

Scattering can occur with or without loss of energy. This means that the scattered radiation can have a different wavelength than the incident radiation, such as in Compton scattering[8] (inelastic scattering), or it can have the same wavelength, such as in Rayleigh or Thomson scattering[9] (elastic scattering).
Compton scattering is produced when a photon hits an electron and is bounced away. The photon loses a fraction of its energy, which is taken over by the electron. The process can be compared with one billiard ball colliding with another. The scattered radiation has a different wavelength and has no particular phase relationship (incoherent scattering) with the incident radiation. It cannot produce interference phenomena and therefore does not carry structure information. It is part of the featureless background radiation.

Rayleigh and Thomson scattering[1] happens when photons collide with strongly bound electrons without energy transfer. The electrons start oscillating at the same frequency as the incoming radiation. Due to this oscillation, the electrons emit radiation with the same frequency. Because the emitted waves of neighboring atoms oscillate strictly synchronous to each other, they produce "coherent waves" (coherent scattering) which have the capability to interfere at the detector. These interference patterns carry the information about the particle structure (see 3.4 "Interaction of X-rays with structure").

The efficiency by which X-rays are scattered depends on the amount of electrons per illuminated material volume. Every illuminated electron contributes the same amount of scattered radiation, which is expressed by the so-called "scattering cross-section", $\sigma = 7.93977 \cdot 10^{-26}$ cm^2 or Thomson factor. It is the scattered energy that is produced by an incident beam of unit energy per unit area. The scattering cross sections of atoms can be found in tables[10].

➤ 3.3. Detection of X-rays

X-rays are detected by methods using an absorption process in the first step. Solid-state detectors, gas-filled detectors and scintillation detectors all use the fact that free electrons are produced due to the impact of an X-ray photon, which will be absorbed in this impact. Acceleration, multiplication and amplification processes then lead to electric pulses that are counted and put out as "the intensity" or as "the count rate". Also, imaging plates absorb X-rays and accumulate their energy by excited electrons, the number of which is proportional to the number of photons that hit the imaging plate. Illumination by visible light then makes the excited electrons relax and emit visible fluorescence radiation. This fluorescence is measured with photo-multiplier tubes which are sensitive to visible light.

1. ***Rayleigh Scattering*** *is used, when the incident radiation is visible light.*
   Thomson scattering *ist used in the case of X-rays and neutrons.*

Whatever the type of detector, only the intensity is accessible, i.e., only the squared amplitude of the wave, $I_s = |\vec{E}_s|^2$, and not the amplitude by itself can be measured. Therefore, valuable information about the sign (or the phase) of the electric field is lost. A holographic reconstruction of a three-dimensional structure from recorded intensities becomes practically impossible. Thus, the result of a structure analysis by scattering will always be ambiguous and the data must be interpreted with some knowledge about the sample (e.g., from microscopy or from an understanding of the sample's chemistry).

➤ 3.4. Interaction of X-rays with structure

When X-rays are scattered at atoms, every atom emits spherical waves emanating from the position of the respective atom. Because the outgoing light waves from Thomson-scattering processes are synchronized with the incoming plane waves, they produce interference patterns at the detector's position. The interferences can be constructive (in phase), destructive (out of phase) or somewhere in-between depending on the observation angle 2θ, the orientation and the distance r of the light-emitting atoms from each other.

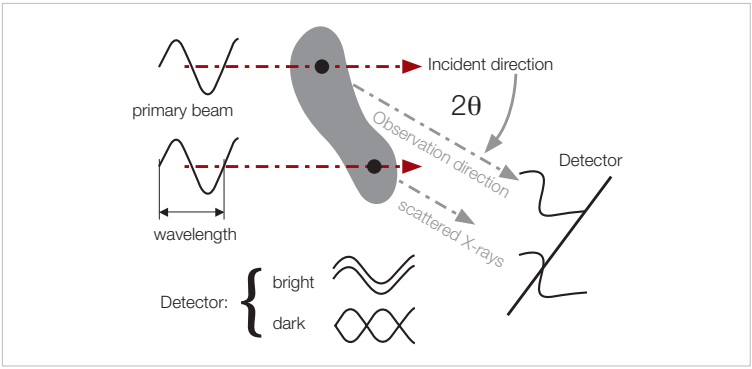

Fig. 3 - 5.

The intensity of interfering waves depends on the distance of the emitting atoms and on their orientations with respect to the directions of incidence and observation. When the waves arrive in phase, the detector receives brightness and when the waves arrive out of phase, then the detector receives darkness.

In a constructive constellation the interference causes a bright spot at the detector and in a destructive constellation the waves extinguish each other, thus producing a dark spot at the detector. The result is a 2D interference pattern, where the intensity varies from position to position in the detection plane (usually measured in terms of scattering angle 2θ and azimuth angle ϕ). The interference pattern is characteristic to the internal structure of the material, i.e., to the orientation and distances of the atoms relative to each other.

Every distance is measured relative to the wavelength λ of the applied radiation. An identical interference pattern is therefore produced whenever the ratio r/λ is identical. In an attempt to become independent from the wavelength, scattering patterns are usually presented[2] as functions of q,

$$q = \frac{4\pi}{\lambda} \cdot sin(\phi), \qquad [1/nm]$$

Names for q, which can be found in literature, are “length of the scattering vector” or “momentum transfer”. Whatever the name, fact is that the dimension of q is one over length (e.g., [1/nm]) and this explains that a scattering pattern is usually called “the structure in reciprocal space”, whereas the particles are said to have a “structure in real space”, because they can be measured in units of length (e.g., [nm]).

2. *Some authors prefer to use $s = \frac{q}{2\pi}$ instead of q, because of its convenient application in crystallography. Its reciprocal value directly gives the distance between crystalline lattice planes.*

➤ 3.5. The form factor

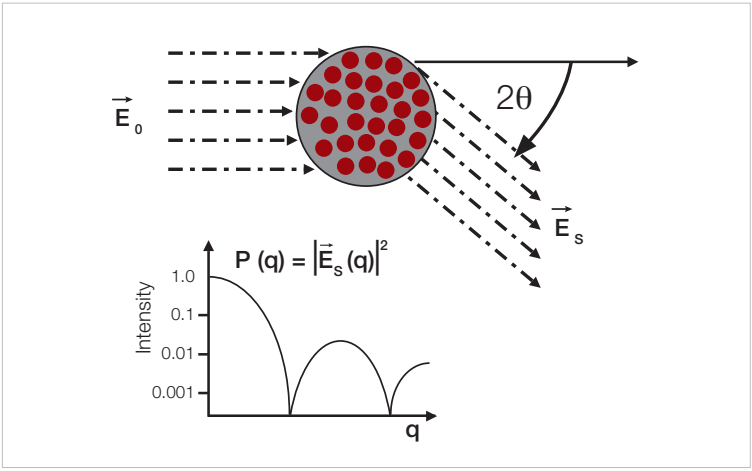

Fig. 3 - 6.

The form factor, P(q), of a particle is an interference pattern, the oscillations of which are typical of the particle's shape.

The scattering of one particle, which is made of many atoms, can be explained as the interference pattern produced by all the waves that are sent to the detector from every electron/atom inside the particle (see Fig. 3 - 6.). Summing up all the wave amplitudes at the detector position and making the square of this sum results in an interference (scattering) pattern. This pattern oscillates in a fashion that is characteristic for the shape (or the form) of the particle. It is therefore called "the form factor". It is a "factor", because it must be scaled with a constant in order to match the experimental intensity units. For structure determination the scaling factor is not required.
In practical applications many particles are illuminated at the same time and the observed scattering pattern corresponds to the form factor of one particle only,

1. if the particles are all identical in shape and size (i.e., monodisperse sample) and

2. if the particles are far away from each other (i.e., dilute sample).

If the sample is dilute, then the form factors of all illuminated particles can be summed up. In a dilute sample the experimental scattering pattern is the form factor multiplied by the number of particles that are in the X-ray beam.

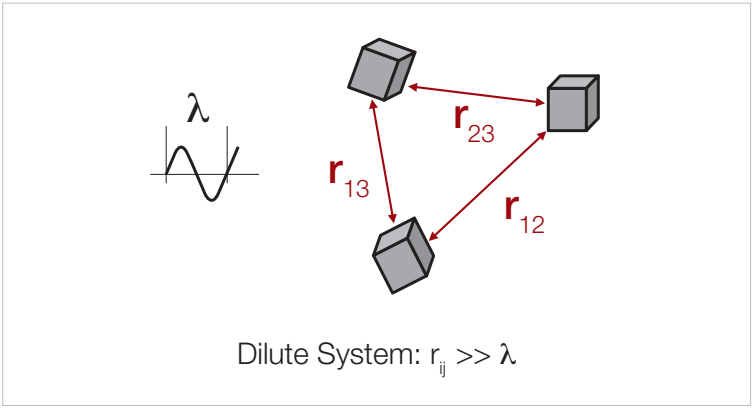

Fig. 3 - 7.

A dilute system of particles is defined for SAXS, when the distances between the particles are large in comparison to the wavelength λ.

If the particles have different sizes (e.g., polydisperse samples), then the form factors of all particle sizes are summed up to obtain the average scattering pattern of the whole sample. Because every size produces form factors with their minima at different angles, the sum of all form factors will no longer contain well-determined minima. We discuss this in more detail in 3.9 “Polydispersity” below.

➤ 3.6. The structure factor

When particle systems are densely packed (i.e., concentrated samples), the distances relative to each other come into the same order of magnitude as the distances inside the particles. The interference pattern will therefore contain contributions from neighboring particles as well.

This additional interference pattern multiplies with the form factor of the single particle and is called “the structure factor”. In crystallography it is known as “the lattice factor”, because it contains

the information about the positions of the particles with respect to each other. Concentration effects become visible at small angles by the formation of an additional wave (see Fig. 3 - 8.). The descent in intensity at small q-values is typical for repulsive interaction potentials. An intensity increase indicates attractive interaction, which is very similar to aggregation.

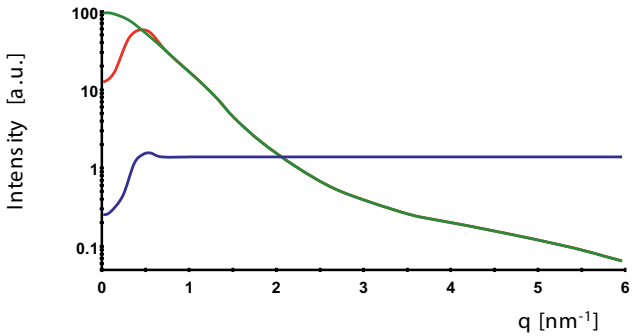

Fig. 3 - 8.

The SAXS profile of (red) a concentrated particle dispersion is the product of (green) the form factor of the single particle with (blue) the structure factor of the particle positions.

Eventually this wave can develop into a pronounced peak, when the particles align themselves into a highly ordered and periodic (i.e., crystalline) arrangement. It is then called a Bragg peak and the position of its maximum (q_{Peak}) indicates the distance (d_{Bragg}) between the aligned particles by using Bragg's law:

$$d_{Bragg} = \frac{2\pi}{q_{Peak}}, \qquad [nm]$$

➤ 3.7. Orientation and order

In a densely packed particle system the positions and orientations of its particles can align themselves with respect to each other. This is usually summarized by the expression “interaction”. For example, the molecules of a liquid cannot move freely, because they cannot penetrate each other. The particle-particle repulsion (among other inter-particle forces) leads to a so-called short-range order. This means that there is an increased probability to find a next-neighbor particle at a specific distance. At larger distances, however, the relative positions become more and more random to each other. The result of this short-range order is the build-up of a structure factor in the SAXS pattern.
The peaks in the structure factor become more and more pronounced, when the particle positions become increasingly ordered. When the domain size of ordered particles increases (i.e., formation of long-range order), the system is said to crystallize. The structure factor of a crystalline substance is normally called lattice factor. It is a set of narrow and intensive peaks at well-defined angles indicative for the crystal symmetry. It can be shown that the ratios of the peak positions on the q-scale have typical values, which reveal the crystal symmetry. For example,

1. Lamellar symmetry: 1, 2, 3, 4, 5, ...
2. Cubic symmetry: 1, √2, √3, 2, √5, ...
3. Hexagonal symmetry: 1, √3, 2, √7, 3, ...

In addition to this positional order, the particles can also develop a preferential orientation with respect to each other, especially when the particle shapes are not spherical. The alignment of particle orientations is only partial in sheared or stretched samples, but it is perfect in crystalline samples.

Orientation and its degree can be observed in a 2D scattering pattern by the amplitude of intensity modulation, when measured in a circle around the primary beam. When the sample is randomly oriented (isotropic), such as dilute dispersions or crystal powders,

the scattering pattern has equal intensities along concentric circles around the incident beam (see Fig. 3 - 9.). It shows intensity modulations when the sample is partially oriented, such as in sheared liquids or spun fibers. When the sample is a single crystal in a specific orientation with respect to the incident beam, then this is signalized by intensive spots (reflections).

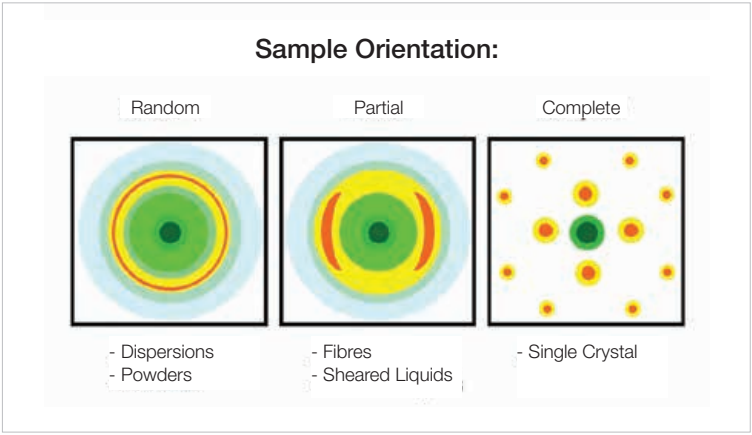

Fig. 3 - 9.

The 2D scattering patterns of randomly oriented (isotropic), partially oriented and perfectly oriented (single crystal) samples.

➤ 3.8. Intensity and contrast

In order to compare theoretical with experimental scattering curves, one can scale the theoretical ones (form factor and structure factor) by arbitrary constant numbers. These scaling factors contain no information about the shape of the particles and, thus, can be chosen arbitrarily. Occasionally, however, they gain a certain interest, when particle number densities or molecular weights of particles have to be determined, as discussed later (see „Molecular weight“ on page 67).

X-rays are scattered by electrons. The scattered intensity of one electron (the “scattering cross-section”) is a constant,

$\sigma = 7.93977 \cdot 10^{-26}$ cm^2 . It is the scattered energy that is produced by an incident beam of unit energy per cm^2. If it is illuminated by a beam of energy density i_0 [a.u. / cm^2], then the resulting scattered intensity

is $i_0 = i_0 \cdot \sigma$ [a.u.], where “a.u.” means arbitrary detector units. It can be “counts per second”, Joule or even Watt, depending on the read-out capabilities of the detection device. The intensity arriving at the detector is modified, however, by the sample transmittance T, the sample-detector distance R, the size of the detection area (pixel size) A and by the polarization angle φ of the incident waves relative to the plane of observation (see Fig. 3 - 10.).

$$I_0 = i_o \cdot \sigma \cdot \frac{A}{R^2} \cdot T \cdot [(sin\varphi)^2 + (cos\varphi)^2 cos(2\theta)^2], \qquad [a.u.]$$

X-rays of standard laboratory sources are randomly polarized, which amounts to $\varphi = 45°$ (averaged polarization). At synchrotrons the polarization angle can have any value between $\varphi = 0°$ (horizontal polarization) and $\varphi = 90°$ (vertical polarization). In SAXS experiments, i.e. for ($2\theta < 10°$), the polarization term is usually ignored, but not in XRD experiments.

The more electrons are placed in a sample volume (i.e., the higher the electron density), the more waves are scattered. If the sample is just one particle of volume V_1 with an electron density of ρ_1, then $V_1\rho_1$ wave amplitudes are scattered. The detector read-out (i.e. the intensity) is the square of all wave amplitudes that come from this volume. The total scattered intensity of this particle $I_{1\,(q)}$ then amounts to

$$I_1(q) = I_0 \cdot \rho_1^2 \cdot V_1^2 \cdot P(q), \qquad [a.u.]$$

where P(q) is the form factor of the particle.

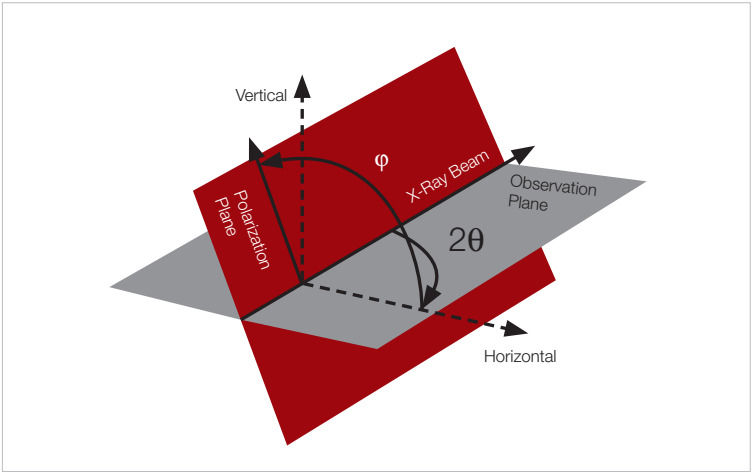

Fig. 3 - 10.

The polarization angle φ defines the angle between the plane in which the radiation wave oscillates (i.e., the polarization plane) and the plane in which the scattering angle 2θ is measured.

Only the interfering photons carry information on the structure.The scattering of the matrix material also carries information but on a much smaller length scale (on atomic distances). It just causes a flat radiation level (background) in the SAXS region and can equally well be set to zero. In practice, one subtracts the blank scattering (of sample holder and matrix) from the sample scattering.

Particles embedded in a matrix material must have an electron density different from that of the matrix in order to become visible in SAXS. The visibility increases with the difference in electron density between the two materials. This is called contrast. If the electron density of the particles were the same as the electron density of the matrix (see Fig. 3 - 11.), then the particles could not be distinguished from their environment and the SAXS signal would be just the same as that of the background.
Measures to exploit the effects of contrast are called “contrast variation”. By changing the electron density of the solvent, some particle components can be made invisible. By incorporating heavy-metal ions into formerly invisible particle components, they can be made visible. In some cases contrast variation is not

possible without destroying the sample structure, because changing the solvent composition or staining with heavy-metal ions is an invasive process. In such a precarious situation SAXS will not be of great use. Instead one could use small-angle neutron scattering[5] (SANS) instead. SANS is a paragon of contrast variation owing to the enormous contrast difference between hydrogen and deuterium. Another method to help out from low-contrast situations would be anomalous small-angle X-ray scattering[11] (ASAXS), which measures the scattering pattern at two different wavelengths. One of them close by the absorption edge of a particular atom, which then gains in contrast considerably. Both methods, however, are only possible at large-scale facilities, such as atomic reactors or spallation sources (to get neutrons) or synchrotrons (in order to tune the wavelength).

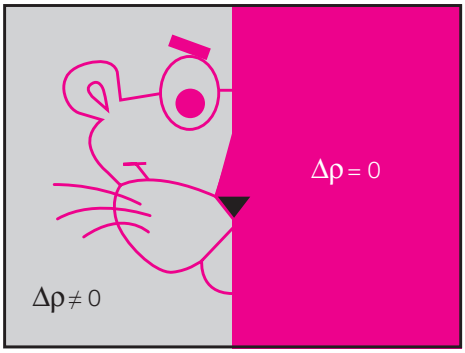

Fig. 3 - 11.

The contrast in SAXS is the difference of electron densities (shown as pink color) between particle and environment. A pink panther in a pink room is invisible with the exception of the nose which remains visible due to its non-zero contrast.

When a particle with the electron density of ρ_1 is embedded into a matrix of electron density ρ_2 , then the scattered intensity of the particle is

$$\Delta I_1(q) = I_0 \cdot (\Delta\rho)^2 \cdot V_1^2 \cdot P(q), \qquad [a.u.] \tag{1}$$

where $\Delta\rho = \rho_1 - \rho_2$, because the intensity of the matrix is already subtracted.
An ensemble of identical particles consequently causes an intensity of

$$\Delta I_(q) = N \cdot \Delta I_1(q) \cdot S(q), \qquad [a.u.] \tag{2}$$

where S(q) is the structure factor considering the particle positions relative to each other. In the case of a dilute system, the approximation S(q) = 1 holds.

One consequence of Eq.(1) is that the SAXS signal increases strongly with the particle volume. Because the volume of a spherical particle increases with the third power of the radius, the SAXS signal increases with the sixth power of the particle radius. Consider a dispersion that contains one million particles of 1 nm radius and just one particle of 10 nm radius (i.e., 1 ppm of the bigger particles). This sample will produce a scattering pattern with equal amounts of intensities from both sizes. You will have to record many electron-microscopic pictures in order to find this one big particle!

The other consequence of Eq.(1) is that the squared contrast is responsible for the SAXS signal. This means that the sign of the contrast has no effect at all. Voids in a matrix material give the same intensity as material particles in a void matrix. It is solely to the judgment of the experimenter, which parts of the sample are considered “particles”.

➤ 3.9. Polydispersity

The assumption that all N particles in a sample are identical is rarely true. Protein solutions are one of the few exceptions of a so-called “monodisperse” sample, where all particles have the same size and the same shape. Usually the sample particles have all different sizes, which is called “polydisperse” or have different shapes, which is called “polymorphous”.

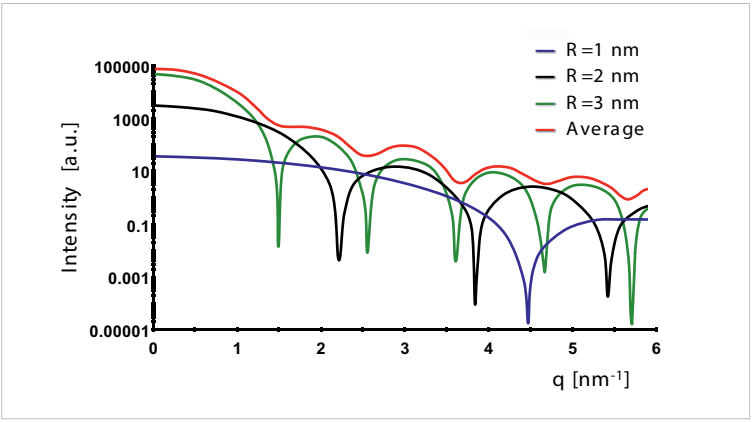

Fig. 3 - 12.

The sum (red) of the form factors of different particle sizes makes the minima vanish gradually.

The scattering curves of polydisperse or polymorphous samples can be regarded as the sum of all N form factors $P_i(q)$, weighted with the respective contrast $\Delta\rho_i$ and volume V_i of the i-th particle. If we assume a dilute particle dispersion (i.e., S(q) = 1), then

$$\Delta I(q) = I_0 \cdot \sum_{i=1}^{N} (\Delta\rho)_i^2 \cdot V_i^2 \cdot P_i(q), \qquad [a.u.] \tag{3}$$

The result of this summation is an averaged form factor, which no longer exhibits sharp minima (see Fig. 3 - 12.). On the other hand, an experimental scattering profile with well-developed minima indicates a monodisperse sample.

➤ 3.10. Surface Scattering

The principles stated in the previous sections are also valid, when the sample is distributed over the surface of a flat substrate and is measured in reflection geometry. Particularly, when the angle of incidence (θ_i) is large compared to the critical angle (θ_c) of the sample (or substrate). The critical angle is the angle below which the sample becomes totally reflecting and the X-rays can no longer penetrate the sample surface. If the angle of incidence is kept close-to-critical (i.e., $\theta_i < 3\theta_c$), then the scattering theory needs additions, because the reflected and the refracted beams (see Fig. 3 - 13.) lead to additional scattering processes, which interfere with particle scattering produced by the direct beam. Scattering curves (GI-SAXS) and reflectivity curves (XRR) in this regime are preferentially modeled with the so-called Distorted-Wave Born Approximation.[15]

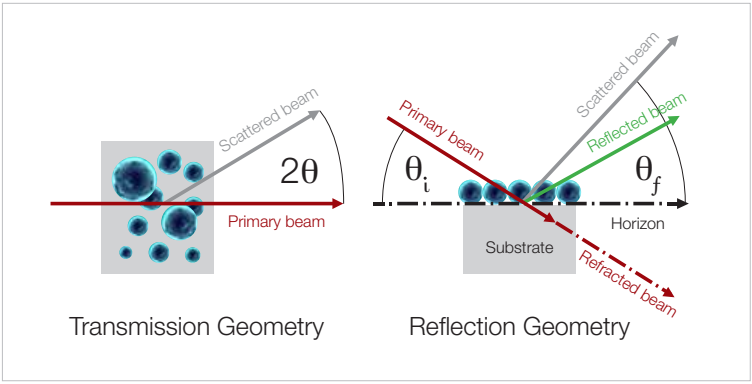

Fig. 3 - 13.

Transmission (left) and the reflection geometry (right) of SAXS experiments. In reflection geometry the detection plane is split up into a refracted (below the horizon) and a reflected scattering pattern (above the horizon). The refracted pattern is rarely observed due to the high absorption of the substrate. The directly-reflected primary beam is the so-called specular beam.

By choosing the incident angle (below or above the critical angle) you can select the depth at which to measure the particles. You can selectively measure surface particles or you can include embedded

particles of buried sample layers. All you need to know is the critical angle of each layer. The critical angle is a material constant, because it is established by the refractive index of the material, $n = 1 - \theta_c^2/2$. It can be calculated[12][13] from the electron density (chemical composition and density) and the absorbance of the sample material. Typical critical angles are between 0.2° to 0.5°.

Reflection experiments always give rise to two superimposed signals. The directly reflected (specular) beam ΔI_{spec} and the diffuse scattering ΔI_{diff}. The specular beam is due to total reflection. As in the case of light being reflected by a mirror, it can be observed in one direction only ($\theta_f = \theta_i$), (see Fig. 3 - 14., red curve). The diffuse scattering is due to surface roughness (or particles) and can be observed at all angles (see Fig. 3 - 14., blue curve).

$$\Delta I_{total}(q) = \Delta I_{spec}(\theta_i) + \Delta I_{diff}(q), \qquad [a.u.]$$

In reflection geometry the definition of has a slightly different appearance,

$$q = \frac{2\pi}{\lambda}[sin\theta_i + sin\theta_f], \qquad [1/nm]$$

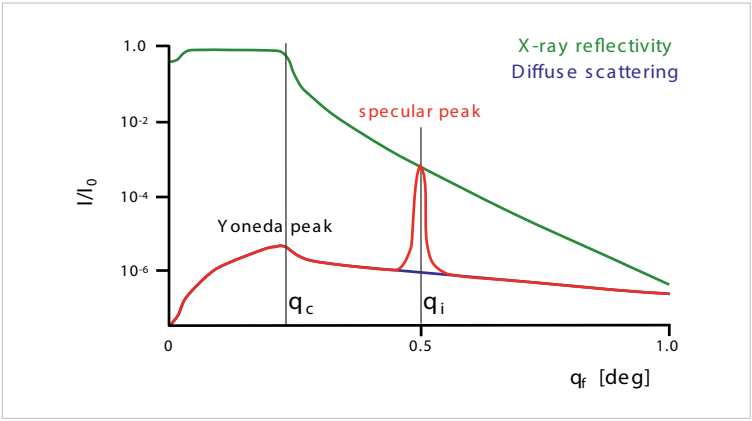

Fig. 3 - 12.

Profiles of a plain surface as obtained (green) by XRR in reflectivity mode ($\theta_f = \theta_i$) and (blue+red) by GI-SAXS in diffuse scattering mode (θ_i = const).

Depending on the way of how the angles θ_i and θ_f are chosen, we find three methods commonly used to characterize surface-near structures.

1. **X-Ray Reflectivity (XRR):** In this experiment the detection angle is always the same as the incident angle, $\theta_f = \theta_i$. Both angles are scanned simultaneously. Only the directly reflected beam is recorded. The quantity of interest is the density profile along the surface normal. So, layer thickness is the main topic addressed by XRR. Surface roughness reduces the reflected beam intensity by increasing the diffusely scattered intensity. Strong roughness can make XRR experiments impossible.

2. **Grazing-Incidence SAXS (GI-SAXS) and Diffraction (GID):** In these experiments the angle of incidence is kept constant and close to the critical angle, θ_i = const $\approx \theta_c$, and the detection angle is arbitrary in one or two dimensions. The magnitude of the detection angle determines, whether it is a small or a wide-angle (i.e., diffraction) technique. The specular direction is sometimes avoided due to the overlap with the intense specular reflection (when $\theta_i \approx \theta_c$). This method scans for lateral structures/particles/roughnesses which are spread over the surface or are embedded in the surface layer of the sample. It is complementary to XRR, because its intensity increases with surface roughness. If

the surface roughnesses of neighboring layers are correlated, then even the surface thicknesses can be determined as is preferentially determined by XRR.

3. **Constant-q Experiment (Rocking-Curve Scan):** This is a variant of the GI-SAXS method by which the sum of incidence and detection angle is kept constant, $\theta_f + \theta_i = \text{const}$, i.e., only the sample rotates, while detection and source direction remain constant. It is used for the same purpose as GI-SAXS, but the accessible particle sizes are much larger (due to the small x-component of the scattering vector, see „Data interpretation in reflection mode“ on page 81) and the surface structures are sampled along the beam direction rather than in the lateral direction.

The advantages of these methods lie in their intrinsic property of sampling large surface areas simultaneously due to the small incident angles.

Scattered and reflected waves interfere at the detector and give additional features, which are not observed with ordinary SAXS.

1. The most prominent feature is the so-called Yoneda peak (see Fig. 3 - 14.). It is produced by surface waves (which are induced by the refracted beam) and it appears always at the critical angle away from the surface horizon, i.e. $\theta_{Yoneda} = \theta_i + \theta_c$ as measured from the direction of the primary beam. Every layer in the sample with a different electron density gives its own Yoneda peak, provided that the layers above can be penetrated at the chosen angle of incidence.

2. In contrast to the Yoneda peak, the directly reflected beam (i.e., the specular peak) appears in a GI-SAXS profile always at twice the incident angle $\theta_{spec} = 2\theta_i$ (see Fig. 3 - 14.).

Both (peak) intensities depend on the Fresnel reflectivity coefficients of the sample as described by S.K. Sinha[15] for a single surface. The intensities of multiple rough layers were calculated by V.

Holy et al.[17][18] The diffuse scattering of many particle systems on surfaces were implemented by R. Lazzari[19] in a simulation and fitting program called IsGISAXS. A good overview and details about surface scattering with X-rays is given in the book of M.Tolan[14] and shall not be repeated here.

4. The SAXS instrument

The basic components of all SAXS instruments are a source, a collimation system, a sample holder, a beam stop and a detection system. The source irradiates the sample, and the detector measures the radiation coming from the sample in a certain range of angles. The collimation system makes the beam narrow and defines the zero-angle position. The beam stop prevents the intensive incident beam hitting the detector, which would overshadow the relatively weak scattering of the sample and would even destroy some of the detectors.

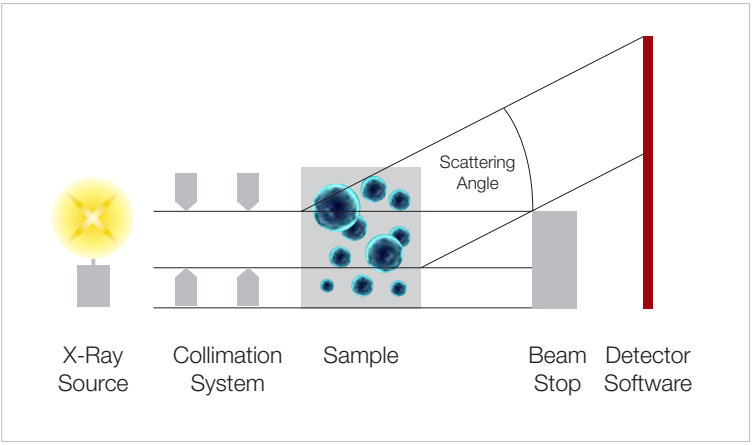

Fig. 4 - 15.

The components of a SAXS instrument.

➤ 4.1. The X-ray Source

In most cases the source is is a sealed X-ray tube, a microfocus X-ray tube or a rotating anode. Alternatively synchrotron facilities are employed in order to have a higher photon flux or when different wavelengths are required.

4.1.1 Sealed X-ray tubes

The basic design of an X-ray tube is shown in Fig. 4 - 16. It contains a filament (wire) and an anode (target) placed in an evacuated

housing. An electrical current heats up the filament so that electrons are emitted. Some high voltage (around 30 - 60 kV) is applied across the filament and the anode, so that the electrons are accelerated towards the anode.

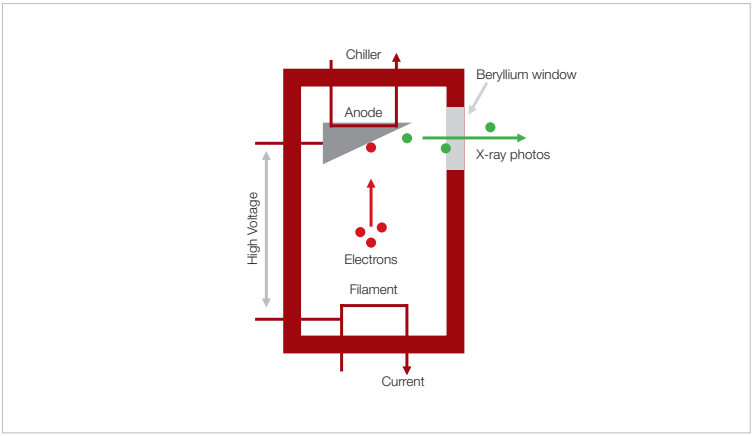

Fig. 4 - 16.

The basic design of a sealed tube.

When the electrons hit the anode they are decelerated, which causes the emission of X-rays. This radiation is called Bremsstrahlung (German for deceleration radiation) and it is a broad spectrum of wavelengths with energies not exceeding the applied high voltage (e.g., 40 kV limits it to 40 keV). A fraction of the electrons will expel electrons from the atoms of the anode. An internal rearrangement of the remaining electrons then causes emission of characteristic fluorescence radiation with wavelengths typical for the material of the anode (for SAXS mostly copper).

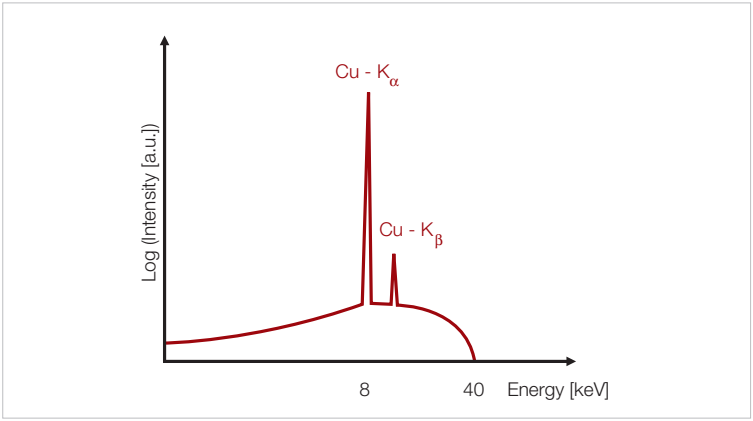

Fig. 4 - 17.

The emitted wavelength spectrum of a copper tube operated at 40 kV.

The intensity of the X-ray tube (i.e., the number of photons) is controlled by the number density of electrons (current) that hit the anode. Usually the copper tubes are operated with 2 kW, which can be achieved by setting the high voltage to 40 kV and the electron current to 50 mA.

4.1.2 Rotating anodes

The bombardment of the anode material with electrons causes aging effects. These are basically grooves or holes, which are burned into the anode material and finally lead to a break-down of the X-ray tube. In order to enhance the lifetime of the source, the anode can be made into a rotating wheel. The bombardment of the anode is then distributed over the whole circumference of the wheel and the reduced wear per area increases the life time or enables higher power settings. People choose this type of X-ray source mostly to increase the electron current and thus the intensity output. The photon flux of a rotating anode can be up to 10 times higher than that of a sealed tube. But also the maintenance costs are 10 times higher than that of a sealed tube. In addition, the work load to keep the anode chamber clean enough to obtain a high vacuum definitely requires permanently employed staff.

4.1.3 Microsources

Recently microfocus X-ray sources became available for SAXS applications. In these sources the electrons are focussed into a small spot on the anode. The X-rays therefore are emitted from a small area of about 20 to 50 µm in diameter. This facilitates the production of narrow beam profiles for point-collimation experiments (see „The collimation system“ on page 39). Because of these small beam dimensions, unnecessary photons are spared, which would not go through a narrow slit or pinhole system anyway. Microsources are therefore very cost effective for point-collimation experiments. Usually microsources are powered with 30 to 50 watts, so that an ordinary water circulator or even air cooling is sufficient to operate them.

About the same photon-flux density (called brilliance) can be achieved as with a 2 kW sealed tube source connected to the same point-collimation system due to the efficient X-ray production. However, high-flux applications are still better done in line-collimation. For these a low-power microsource is just too weak.

4.1.4 Synchrotron radiation

Synchrotron facilities provide X-rays of all wavelengths as a by-product of forcing charged particles (electrons or positrons) to move along a circular (or wiggly) path at high speed. This process produces Bremsstrahlung and therefore a continuous wavelength spectrum is available. The power consumption of a synchrotron facility is enormous and the photon flux is accordingly. Because the charged particles are moving in bunches, the synchrotron radiation is a pulsed source. The intensity from a synchrotron is not constant over time. It decays due to the dissipation of charged particles, and it needs to be refreshed by injecting new particles from time to time.

At almost every synchrotron one or more beam lines are available for specially dedicated experiments such as SAXS. Projects must be formulated and applied for at the synchrotron stations. After a reviewing process and upon acceptance the applicant is granted a time slot from a few hours to a few days once or twice per year. Usually those applicants are favored for acceptance, who can show that high flux is mandatory for the success of their experiments and that previous screening experiments (e.g. with laboratory instruments) have indicated that their samples are suited for the synchrotron application.

➤ 4.2. The collimation system

In SAXS the biggest challenge is to separate the incoming beam from the scattered radiation at small angles (around <0.1°). If the incoming beam has a larger divergence than this small-angle requirement, then it becomes hard to distinguish the relatively weak intensity of the scattering pattern from the much higher intensity of the direct beam. Therefore the divergence of the incoming beam must be kept small.

Hence, a collimation system is required. This is basically a system of slits or pinholes, where the beam has to pass through. In order to make the beam narrow, the slits or pinholes must be very narrow and far away from each other. But this cuts down the intensity of the incident beam considerably. As a trade-off one allows the slit or pinhole size to be larger than zero, but at the cost of instrumental broadening of the results, called slit smearing.

Usually the X-rays that are emitted by the source are polychromatic, that means they are a mixture of photons of different wavelengths. A sample that scatters the photon of one wavelength into one specific direction (angle) will scatter the photon of another wavelength into a different direction. Polychromatic radiation is therefore another cause for instrumental broadening, called wavelength smearing.

In order to prevent wavelength smearing, multilayer optics can be can be used to monochromatize the beam. These optics diffract X-rays of only one particular wavelength λ according to Bragg's law, $n\lambda = 2d \sin(\theta/2)$, with a typical multilayer d-spacing of about 4 nm. The wavelength can be selected by tilting the multilayer by an angle with respect to the direction of the incident beam. The integer θ indicates that also n-times shorter wavelengths can pass through, but these are suppressed by the special design of the multilayer mirror.

SAXS instruments are normally classified in two categories according to the collimation system employed.

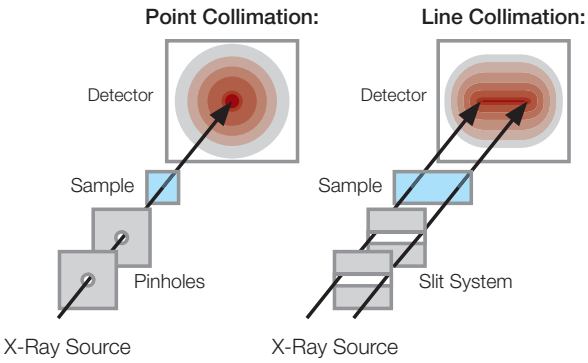

Fig. 4 - 18.

The two collimation systems used in SAXS instruments.

(1) Point-collimation instruments have pinholes that shape the beam to a small circular or elliptical spot. Only a small spot of the sample is illuminated. The beam dimensions at the sample position are typically 0.3 x 0.3 mm^2. The scattering is therefore centro-symmetrically distributed around this illuminated spot and the 2D pattern in the detection plane consists of concentric circles around the primary beam (Fig. 4 - 18.). The scattering patterns

have only little slit smearing, which is mostly neglected in subsequent data evaluations. However, at small angles this slit smearing can become evident and non-negligible even with point-collimation systems.

Owing to the small illuminated sample volume the scattered intensity is small. It is also very difficult to obtain a narrow and clean beam with a point-collimation set-up, which generally results in poor resolution (see 5.4.1 “The resolution” about the definition of resolution). Mostly the resolution can be improved a bit by increasing the sample-to-detector distance. But this makes the instruments large (up to a few meters) which diminishes the intensity at the detector. Therefore the measurement time with point-collimation systems is in the order of hours.

Point-collimation instruments are indispensable whenever orientation distributions have to be investigated (Pole Figure, RheoSAXS), when small sample areas (Microdiffraction) or surface properties (GI-SAXS) are to be investigated.

(2) Line-collimation instruments confine the beam only in one dimension, so that the beam profile is a long but narrow line with dimensions of typically 20 x 0.3 mm^2. The illuminated sample volume is much larger than in point collimation (about 50 to 100 times) and the scattered intensity (at the same flux density) is therefore bigger by the same amount. The beam profile can be made much narrower and much cleaner than with point collimation, so that a small sample-to-detector distance can be exploited to the full. This has the consequence that the intensity is larger by another factor of about 10 (due to the $1/R^2$-dependence of the scattered intensity, see „Intensity and contrast“ on page 24). The measurement time is therefore some 100 times shorter than with point-collimation setups.

The large sample volume however causes substantial broadening (slit smearing) of the scattering pattern (see Fig. 4 - 18.), so that the beam profiles must be measured and incorporated into

the data evaluation. Slit smearing becomes increasingly negligible with larger scattering angles, so that the benefit of high intensity is not compromised in the wide-angle region. At smaller angles the smearing effect can be eliminated by an additional mathematical treatment, called “desmearing” (see „Correction for collimation and wavelength effects“ on page 57). This can be performed with several software packages.[20]-[22]

Line-collimation instruments are ideally suited for non-oriented (= isotropic) systems, such as diluted dispersions and emulsions, and for the screening of large sample volumes.

➤ 4.3. The sample holder

The most complicated part of a SAXS system is the sample holder. This is because most samples cannot stand the vacuum, which is required to keep background scattering low. Also it is often the change in structure, which is investigated in response to a changing environment or process parameter such as temperature, pressure, flow/shear rate, humidity, strain, projection angle and many others. This huge variety of different parameters makes it impossible to design one general setup, which can make each and every scientist happy. Therefore most sample holders are either completely homemade or are variants of commercially available setups. We cannot ignore the importance of a suitable sample holder but we have to limit our efforts by mentioning only the most basic setups in the experimental section below (see „Sample preparation“ on page 48).

➤ 4.4. The beam stop

The function of the beam stop is to prevent that the intensive direct beam hits the detector. Although some detectors are not necessarily destroyed by high intensities, the strong backscatter from the detector material can overshadow the relatively weak signal from the sample.

Two different types of beam stops are in use. One type consists of dense materials, such as lead or tungsten, which blocks off the direct beam completely. The other type is made of transparent materials which attenuate the beam to an intensity level that can be handled safely by the detector.

The advantage of a transparent beam stop is that the intensity of the direct beam is monitored simultaneously with the sample scattering. Thus, eventual drifts of the generator intensity are easily compensated by normalizing to the same beam intensity. Also the position of the beam and its profile is simultaneously measured in every experiment. Extra experiments to determine the beam-profile and of the zero-angle position are no longer required. However, it must be kept in mind that the material of the transparent beam stop can contribute to the background signal.

The transmitted beam intensity can be used to correct for the absorption of the sample without the need to do extra experiments. However, this absorption correction fails, when strong sample scattering towards zero scattering angle is not negligible (e.g., the scattering of powders).

➤ 4.5. The detector

Four different types of detectors are in use with SAXS. Wire detectors, CCD detectors, imaging plates and solid-state (or CMOS) detectors. Some general specifications of varying importance must be considered when selecting a detector.

1. **Resolution:** It is the ability of the detector to identify two neighboring points (pixels) as separated. A high spatial resolution means that the detector has many pixels per length and that the cross-talk between the pixels is negligible. Cross-talk between pixels happens, when the intensity of one pixel to a certain degree spreads to neighboring pixels. A high resolution is important for small SAXS instruments.

2. **Linear dynamic range:** It is the range of photon flux which can be converted into exactly proportional intensity values. Usually detectors become less sensitive towards higher flux (called detector saturation). This means that an increase of photon flux by a factor of two does not lead to an increase of the recorded intensity by the same factor. Integrating detectors can add to their linear dynamic range by their high precision.

3. **Precision:** It is the accuracy and stability of the read-out intensity values. If still significant signal remains after subtraction of a background of similar intensity, then the precision is high and additional decades of linear dynamic range are gained on the low intensity side. If only noise remains, then the precision is poor. Every SAXS measurement requires two experiments which then must be subtracted. This is therefore an important specification for SAXS.

4. **Sensitivity:** It indicates how efficiently incoming photons are counted. It is measured in quantum efficiency (QE) values, i.e., the percentage of photons that are effectively counted. QE goes hand in hand with the absorption of the detector medium. Because most detectors nowadays have QE-values at around 90% (with the exception of wire detectors, which have about 60%), little can be improved on this side. It is a less important specification for SAXS, unless a shorter wavelength than copper radiation is used.

5. **Dark-count rate:** It is the intensity that the detector records even though no X-ray beam is switched on. It is mostly attributed to thermal processes and can be removed by cooling the detector or by filtering the electrical pulses according to their height. (The pulse height that is produced by the photon is directly related to the wavelength of the photon. It can be used to selectively count only those pulses that have a particular wavelength.) Detectors with a substantial dark-count rate must have a high precision in order to compensate for it.

6. **Frame rate:** It is the number of scattering patterns (pictures) which can be recorded per second. This does not determine the speed of SAXS experiments or the time resolution of so-called “time-resolved SAXS”. The speed is rather determined by the number of scattered photons per second. In order to obtain a scattering pattern in an acceptable quality, a sufficient number of photons must be recorded. So, the bottleneck is not the frame rate of the detector but the number of the scattered photons per second. The frame rate is a less important specification for SAXS.

4.5.1 Wire detectors

These have thin wires inside an absorbing gas atmosphere (Xe or Ar/Methane). One X-ray photon that enters this atmosphere expels an electron from the gas molecules. The electron is accelerated towards the wire by the applied high voltage (bias). When the electron hits the wire an electrical pulse is induced inside the wire. The pulse propagates towards both ends of the wire, where its arrival is recorded. The time difference between the two arrivals is used to determine the position where the electron hit the wire. One wire is capable of delivering a 1D scattering profile and many wires running parallel can be used to produce a 2D picture.
Wire detectors usually have large pixel sizes (around 100 µm) and therefore have a poor spatial resolution. A larger sample-to-detector distance can be a cure for this, but only at the cost of a diminished angular range and a reduced intensity. The advantage lies in their ability to filter pulses according to their wavelength, resulting in a negligible dark-count rate. Wire detectors can be easily damaged by overexposure and are costly to maintain.

4.5.2 Charge-coupled device (CCD) detectors

CCD cameras work like ordinary video cameras. They detect visible light, which is produced by a fluorescence screen. A plate made

of glass fibers, a so-called taper, is mounted between the video chip and the fluorescence screen. It guides the light to the chip and maps the fluorescence pattern with little distortion. A Beryllium window or an Aluminum-coated plastic foil prevents that ambient light spoils the detection of the comparatively weak fluorescence. The CCD is an integrating detector, i.e., it collects the produced electrons in every pixel (=capacitor) until read-out. Only the resulting charge is recorded and not the photon impact itself. This has two important consequences. First, the noise amplitude of a CCD detector is not the square root of the recorded intensity (i.e., no Poisson statistics, see „Exposure time“ on page 51). Second, no filtering of pulses is possible to eliminate the dark-count rate. So, CCDs need efficient cooling (e.g., water circulators) to keep the dark-count rate as low as possible. The dark-count rate also depends on the acquisition time, so that it has to be measured quite frequently (instead of once-and-for-all). Fortunately, the CCDs are equipped with the capability of on-chip binning. This feature connects neighboring pixels and thus increases the precision considerably. Usually the pixel sizes are small (around 25 µm) and the cross-talk affects hardly more than three neighboring pixels, so that high-resolution experiments are possible. High-intensity spots, however, can lead to blooming (i.e., extreme cross-talk over the whole chip width), which calls for corrective actions after the acquisition (so-called anti-blooming correction). The chip sizes are relatively small (max 5x5 cm), which limits the angular range. The prices of CCD cameras are relatively high and depend on the chip quality (which is specified by the number of failing pixels).

4.5.3 Imaging plate detectors

Imaging plates are made of a material that stores the X-ray energy by exciting its electrons into so-called F-traps. These are meta-stable energy states from which the electrons can be brought back by illumination with a laser beam. Thereby visible fluorescence radiation is produced, which is measured by a photo-multiplier or an avalanche photodiode. Imaging plates are flexible sheets which are exposed just as photographic films and are scanned by a separate

device in a second step. After the readout (digitization), the imaging plates are cleared by a light-pad before they can be used again. They can be reused many 1000 times until mechanical damage causes the end of their life. Imaging plates have have a comparably high linear dynamic range and they can be produced in virtually any shape and size. But they usually need to be scanned by an external device, which makes automated experiments difficult. Imaging plates must be handled in darkened labs, because illumination with ambient light leads to uncontrolled erasure of the scattering pattern. The dark-count rate depends on the scanner model (used photomultiplier) but is usually small, constant and easy to subtract. Also the pixel size depends on the scanner model and lies typically between 25 and 100 µm. The pixel cross-talk, however, is substantial. The plates have almost no maintenance costs and they are not easily damaged by overexposure. It is the ideal detector for teaching purposes.

4.5.4 Solid state (CMOS) detectors

Solid state detectors are Si-diode arrays (1D and 2D) which record the X-ray photons directly. When X-ray photons hit the semiconductor material, they produce ion pairs which are actually counted. Additional circuitry (op-amps) then selectively counts only those pulses that are above a certain energy threshold. In this way the dark count rate and also fluorescence of longer wavelengths can be eliminated. Because silicon does not absorb so much short-wavelength radiation, their quantum efficiency reduces substantially, when wavelengths shorter than copper are measured.
They can stand rather high radiation doses and maintain their linearity up to intensities close to that of the primary beam of a 2 kW sealed-tube source. Their radiation hardness is not unlimited, though, because direct-beam intensities (e.g., of a synchrotron) applied for a longer period of time can cause damages, which result in a permanently reduced quantum efficiency. The costs of these detectors are in the same order of magnitude as that of a CCD detector.

5. SAXS analysis

In order to make a good analysis, it is important to have a well-prepared sample and a good data quality. After the sample is measured, the data are analyzed. This is done in various ways and in various extents, depending on the type of sample and on the intent of the investigation.

➤ 5.1. Sample preparation

The SAXS signal can be optimized by employing a large illuminated sample volume (scattering volume).

- **In transmission mode (SAXS):** A thick sample is not desirable due to the increased sample absorption (see „Absorption“ on page 15). So, the only way to maintain a large scattering volume is to widen up the beam dimensions and to keep the optimum sample thickness, which (for water-based samples and copper radiation) is about 1 mm. Typical sample sizes are 50 µL for liquids and 1 x 1 mm^2 (point collimation) to 1 x 20 mm^2 (line collimation) for solid samples or pastes.

- **In reflection mode (GI-SAXS):** The sample thickness is of no concern, because only the topmost surface layers are probed. The only way to maintain a large scattering volume is to increase the sample length. The footprint of a 0.3 mm high beam on a flat sample with an inclination angle of 0.2 degrees is 86 mm. Because half of the beam has to go straight over the sample in order to indicate the zero-angle position, the optimum sample length would be about 40 mm.

Everything that is put inside an X-ray beam, even air, produces scattering. It is therefore good practice to keep the sample-to-detector distance in vacuum. Unfortunately, many samples are destroyed when put into vacuum and need to be kept at ambient conditions. Therefore, special sample holders are necessary to keep the samples fit for the scattering experiments.

5.1.1 Liquids

Liquid samples in transmission mode are measured inside a thin-walled capillary the thickness of which should be around 1mm when the liquid contains mainly water or hydrocarbons. Solvents that contain heavy atoms, e.g. chlorine, and have a large density absorb too much and must be measured in thinner capillaries (see Table 3.1 on page 16). Liquids that are so viscous that, in a lifetime, they could not be filled into a capillary are better measured in a paste cell.

5.1.2 Pastes

Pastes, rubbers, and vacuum sensitive materials in general have to be squeezed into a sample holder that has removable windows. The window material must be transparent to X-rays, should not scatter much and should be resistant to chemical attack and elevated temperatures. The most widely used window material certainly is a foil made of Kapton®. Other window materials are also possible but depend on the requirements of the respective application.

5.1.3 Solids

Solids can be clamped onto frames with or without additional window foils for protection against the vacuum. The sample thickness can and must be chosen according to the respective absorption. In case of special atmospheric requirements, such as a specified relative humidity or a gas reaction, the sample must be put into a small compartment which is then inserted into the vacuum. These can be technically quite challenging and are usually also expensive.

5.1.4 Powders

Powders can be measured between two layers of sticky tape or in (disposable) capillaries. Not every powder is suitable for SAXS investigations, particularly when the grain size or shape is the

desired parameter. With the exception of the specific surface of a powder, only internal structure elements can be found with SAXS. So, the crystallinity on the atomic scale (in WAXS) or on the nanoscopic scale (in SAXS) are the only reasons why one would make scattering experiments on powders. The difficulty with powders, however, is that the grain size must be small enough to allow for a random-enough distribution of crystal orientations. This is necessary to be sure that all Bragg reflections fall into the detection area and thus all peaks are represented in the scattering profile. Not all powders can be ground sufficiently small. Also, sometimes crystals just form in the sample (mostly pastes or liquids) and grow fast enough to spoil the randomness of crystal orientations. In these cases it is a good idea to use a sample holder that rotates or vibrates in such a way that all crystals eventually move into an orientation that allows for their detection within the acquisition time.

5.1.5 Materials on a substrate

Sometimes materials must be prepared on a substrate in order to investigate thin-film properties. Normally one would choose to measure these samples in reflection mode (GI-SAXS). However, if transmission mode is the method of choice (e.g., for pole figure analysis) one has to choose a substrate material which is sufficiently thin and transparent enough for that particular wavelength. If possible, ordinary X-ray window materials can be used. In many cases the scattering of the thin-film is much weaker than the scattering of the substrate, so that a transmission experiment becomes impossible. Again, the thin-films must be able to withstand vacuum conditions. But if they can stand only a normal (or a special) atmosphere, then they must be put into a small compartment that is inserted into the vacuum.

➤ 5.2. SAXS measurements

When the sample is in (or on) the holder the actual measurement can begin. This is done by exposing the sample to the beam. It is important to note that one measurement always consists of two experiments. The scattering of the matrix material (e.g., the solvent) and of the particle system must be measured in two separate experiments. In order to obtain the scattering from the particles alone, one must subtract the scattering of the matrix material.
If the intensities are required in absolute units, then additional experiments are required to calibrate the detector output with a standard material of known output intensity. Please note, however, that absolute intensity units are not required for the determination of a structure.

5.2.1 Exposure time

The statistical quality of the scattering pattern improves with increasing intensity. The standard deviation of the experimental intensity is equal to the square root of the intensity (i.e., law of Poisson statistics). Thus, it is necessary to measure four-times longer in order to reduce the noise by a factor of two. Clearly, a long exposure time is the recipe for data of good quality. On the other hand, long exposure times are not economical and a trade-off solution must be found anew for every sample.
Every detector has a specified saturation value expressed in counts. When this maximum number of counts is reached, then the time that was needed for it constitutes the maximum exposure time for this particular sample. Any further accumulations of counts would be lost in overflows. If the data still need further improvement, it can only be done by repeated exposures and by averaging all the resulting frames. Repeating short exposures is the preferred measuring mode for CCD detectors due to their low saturation value and the missing applicability of Poisson's law, which says that the standard deviations of counted intensities are the square root of the intensity-values themselves.

In practice one determines the optimum exposure time by a short, say, 1 minute long screening experiment. If the interesting parts in the scattering pattern have reached M [a.u.] (arbitrary detector units) in t minutes, then the accuracy (relative standard deviation) of the data is s = 100/ √M %. If the aimed-at accuracy of s_{opt} is not yet reached, then the exposure time must be extended to $t_{opt} = (s/s_{opt})^2$. This rule of thumb applies to all detectors delivering counts as output. For CCD detectors it is still a good approximation.

5.2.2 Contrast

When the contrast between particle and matrix is zero, no prolonged exposure time and no synchrotron with high photon flux will help and make the particles visible. If possible, select a matrix material (solvent) in which the particles have a high contrast. Always try to use a matrix material which is less dense than the particles, or, which is made of lighter elements. This helps to keep absorption losses small, too.

➤ 5.3. Primary data treatment

The distribution of the scattered X-rays is recorded in the plane of detection, which results in a two-dimensional scattering pattern, $I_{exp}(m_y, m_z)$, where m_y and m_z are the horizontal and vertical pixel numbers. Most of the times these are more data than are actually necessary. For example, the scattering of isotropic samples could equally well be described by a one-dimensional scattering profile. Similarly, the orientation angle of an anisotropic sample could be read off from an azimuthal 1D profile. Therefore, the amount of data can be reduced by averaging.

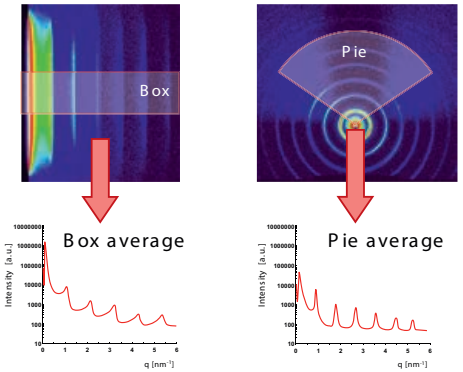

Fig. 5 - 19.

The box geometry (linear average) and the pie geometry (circular average).

There are three geometries (see Fig. 5 - 19. and Fig. 5 - 20.) to average the data, depending on the intent of the investigation and on the collimation type of the instrument.

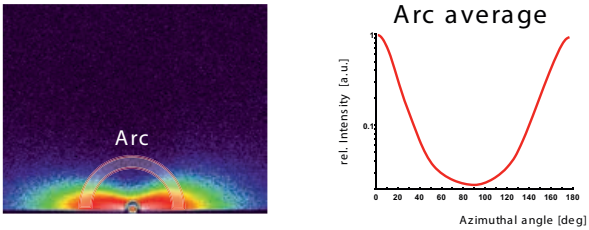

Fig. 5 - 20.

The arc geometry (radial average).

Averaging also improves the statistical quality of the data. It must be done over a certain width, however, which broadens (smears) the profile. This width must be considered in the subsequent data evaluation procedure (see „Correction for collimation and wavelength effects“ on page 57).

The pixel numbers of the profiles are converted into q-values (or azimuth-angle values, ϕ) by taking into account the wavelength,

the pixel size and the sample-to-detector distance. In this way we obtain the 1D profiles $I_{exp}(q)$ and $I_{exp}(\phi)$.

5.3.1 Subtracting the background

What we have obtained so far are two experimental intensity curves, one from the sample $I_{s,exp}(q)$ and one from the matrix material $I_{M,exp}(q)$. Now we need to subtract one from the other, in order to get the scattering of the particles only.

$$\Delta I(q) = I_{S,exp}(q) - I_{M,exp}(q), \qquad [a.u.] \tag{4}$$

This seemingly simple operation cannot always be applied as stated above. It works only, when the sample and the matrix material have about the same transmittance, $T_s = T_M$. The transmittance is the ratio of transmitted versus incident photons. If a material is not absorbing, then its transmittance is 1. So, if the particles in the matrix absorb more than the matrix, $T_s < T_m$, then the scattered intensity of the sample will be reduced. A negligent application of Eq.(4) will then deliver meaningless negative intensities. The experimental scattering curves therefore must be scaled by their respective transmittance values. But before any scaling can be applied, the data must be cleaned from the dark-count rate of the detector, $I_{dc}(q)$. One equation describing this absorption-corrected background subtraction would be

$$\Delta I(q) = \frac{I_{S,exp}(q) - I_{dc}(q)}{T_S} - \frac{I_{M,exp}(q) - I_{dc}(q)}{T_M}, \qquad [a.u.] \tag{5}$$

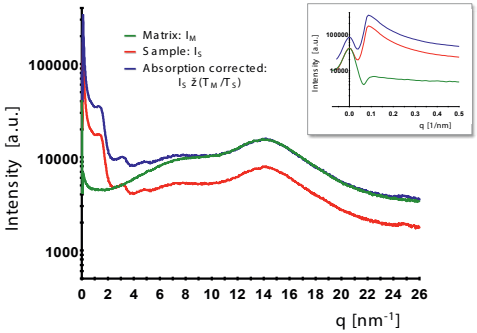

Fig. 5 - 21.

The scattering curve of a dispersion of absorbing particles (red) in a matrix material (green) of low absorbance. Absorption correction brings the sample intensity (blue) slightly above the background intensity (green). The inlet shows the zoomed-out region of the primary beam.

In Fig. 5 - 21. an example is shown, where negative values would result in a subtraction without an absorption correction.

Instead of determining all involved transmittance values, it is more practical though, to determine a scaling factor f_T, which brings the sample intensity above the background intensity. The final equation mostly used is therefore

$$\Delta I(q) = I_S(q) \cdot f_T - I_M(q), \qquad [a.u.] \tag{6}$$

where we have abbreviated, $I_S(q) = I_{S,exp}(q) - I_{dc}(q)$, $I_M(q) = I_{M,exp}(q) - I_{dc}(q)$. The scaling factor is effectively a relative transmittance correction, $f_T = T_M/T_S$, which is alright, if absolute intensity units are not required. It can be easily obtained, when the data reach into the wide-angle region (i.e., q >10/nm^{-1}) and the structure peak of the matrix material (see Fig. 5 - 21. at q = 14/nm^{-1}) is not changed by the presence of the dispersed particles. Just scale the sample

curve by such a factor that a subsequent subtraction does not yield systematically negative numbers, $f_T \cdot I_S - I_M \geq 0$.

Note that the primary beam intensity (see inlet of Fig. 5 - 21.) cannot always be used to find the scaling factor. Some samples scatter strongly towards q = 0. This scattering can compensate the losses due to absorption and the transmission value can no longer be determined by comparing the intensities at q = 0.

Once the obvious background, i.e., the scattering from the sample holder, the matrix material and the dark-count rate of the detector are subtracted, there possibly remains some incoherent scattering (Compton scattering or fluorescence) I_{inc} , which adds a constant to the scattering curve. Its presence can be quickly checked by drawing the background-subtracted data in a double-logarithmic plot.

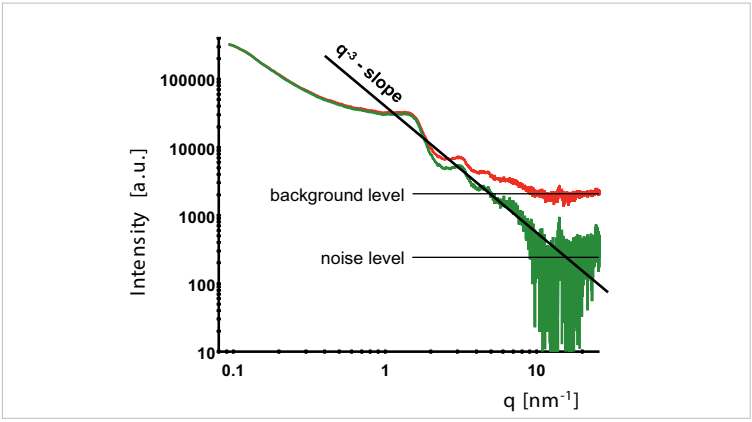

Fig. 5 - 22.

A double-logarithmic plot of data (red) with and (green) without a constant background.

A constant background makes a scattering curve leveling off at large q-values (see Fig. 5 - 22.). Once this constant is subtracted, then the scattering curves should follow a linear slope (of q^{-3} or q^{-4}) down to the noise level according to Porod's law, for point collimation $\Delta I(q) \approx K_P/q^4$ or for line collimation $\Delta I(q) \approx K_L/q^3$.
If the experimental scattering curve contains an unknown amount of constant background , then Porod's law can be used to calculate it by fitting a straight line into a so-called Porod plot of $y = q^4 \Delta I(q)$ versus $x = q^4$ (see Fig. 5 - 23.),

$$q^4 \cdot \Delta I(q) = K_P + B \cdot q^4, \qquad [nm^{-4}]$$

where the slope B = I_{inc}. For line collimation experiments q^3 is used instead of q^4, because of the instrumental broadening.

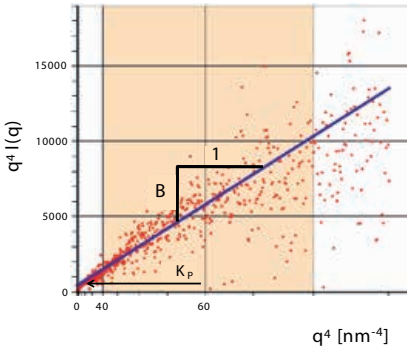

Fig. 5 - 23.

The Porod plot of a scattering profile with a substantial amount of constant background B and the intercept K_P.

5.3.2 Correction for collimation and wavelength effects

All theoretical scattering curves ΔI(q) (form factors and structure factors) which are described in text books are calculated for an ideal primary beam. An ideal primary beam has no length, width and has only one wavelength. In real life, a beam has finite length, width and wavelength profiles. That is the reason why experimental scattering curves ΔJ(q) are broader than the theoretical curves. They are said to be smeared. The most important smearing effect for SAXS is beam-length smearing, when working with line collimation

$$\Delta J(q) = \int_{-\infty}^{\infty} U(t)\Delta I(\sqrt{q^2 + t^2})dt, \qquad [a.u./nm] \tag{7}$$

The beam-length profile U(q) is a trapezoid, which is the measured beam profile additionally broadened by the averaging width of the detector. It can be approximated by a constant value, so that a smeared scattering curve can approximately be regarded as the integral of its theoretical scattering curve, $\Delta J(q) \approx \int \Delta I(q) dq$. This is a very useful result, because it immediately allows translating theoretical predictions into the case of line collimation. For example, Porod's law $\Delta I(q) \approx K_p/q^4$ for line collimation can be calculated quickly, $\Delta J(q) \approx \int K_p/q^4) dq \approx K_p/(-3q^3)$.
Also the inverse operation is possible. It is called desmearing and is effectively the first derivative of the experimental scattering curve. Therefore, also the noise content of an experimental scattering curve is magnified during desmearing.

Desmearing can be done in two ways:

1. **Model-free way**[20]: No assumptions on the scattering system are made. However, no difference is made between signal and noise. Therefore the noise level is equally increased as the waved features of the scattering curve. Longer exposure times can help to compensate the increase of noise. This method is recommended, if Bragg peaks are in the SAXS curve or no suitable fitting model can be found.

2. **Model-dependent way**[21][22]: Theoretical scattering curves of a model are fitted to the data, after they have been smeared with the experimental beam profiles. A fitting procedure automatically separates signal from noise in an effective way, so that the results are always smooth. There is no increase of noise, but having chosen a wrong model can still lead to unacceptable results. This method is recommended, if the SAXS curve can be interpreted in terms of finite pair-distance distributions (see „Particle structure“ on page 69).

Nowadays, for SAXS applications wavelength smearing is history, because multilayer optics make the wavelength distribution of X-ray tubes sufficiently narrow. Neutron scattering applications, however, still have to deal with it.

5.3.3 Intensities on absolute scale

Intensities are called “on absolute scale” if they are normalized by the flux density of the primary beam i_0 [a.u./cm^2] and the illuminated sample volume V_S [cm^3].

$$\Delta I_{abs}(q) = \frac{\Delta I(q)}{i_0 \cdot V_S}, \qquad [1/cm] \tag{8}$$

If the intensities are required in these units (e.g., for molecular-weight determina-tions), then two additional experiments must be made to calibrate with a standard. In these experiments the empty sample holder (e.g., empty capillary) $I_{cap}(q)$ and the sample holder with the reference material (e.g., water) $I_{water}(q)$ are measured. The scattering of the empty sample holder must be subtracted in order to obtain the scattering of the reference material.

$$\Delta I_{water}(q) = \frac{\Delta I_{water}(q) - I_{dc}(q)}{T_{water}} - \frac{I_{cap}(q) - I_{dc}(q)}{T_{cap}}, \qquad [a.u.] \tag{9}$$

If we divide the background-corrected sample intensities by the mean intensity of the reference material, then we obtain them in units of the reference. Once the absolute intensity of the reference material is known (e.g., $I_{water,20°C} = 1.641 \cdot 10^{-2}$ cm^{-1}), the intensities of the sample can be scaled to absolute units [cm^{-1}], too.

$$\Delta I_{abs}(q) = \frac{\Delta I(q)}{\langle \Delta I_{water} \rangle_q} \cdot I_{water,20\,^\circ\mathrm{C}}, \qquad [1/cm] \tag{10}$$

where $<\ldots>_q$ indicates an average value in a q-range, where ΔI_{water} is sufficiently constant. Using water as reference has the advantage that it fills the sample holder evenly and both, i_0 and V_S cancel, when we divide by the intensity of the water filled sample holder. So, Eq.(10) can be readily exploited, if water is the reference. Other reference materials, which are not liquid (e.g., glassy carbon), need a modification of Eq.(10)

$$\Delta I_{abs}(q) = \frac{\Delta I(q)}{\langle \Delta I_{ref} \rangle_q} \cdot I_{ref} \cdot \frac{V_{ref}}{V_S}, \qquad [1/cm] \tag{11}$$

where V_{ref} is the illuminated volume of the reference material. Converting intensities of solid samples into absolute intensity units is complicated, because it is hard to determine the illuminated sample volume precisely.

The method of using reference samples works only, if the intensity I_{ref} is known. In the case of water, it can be calculated theoretically[25]. Other reference materials need to be calibrated and certified, before they can be used. Such a calibration can only be made with an instrument[26] that is capable of measuring the direct-beam flux density i_0 and the scattering of the reference sample under identical conditions.

➤ 5.4. Data interpretation

Once the intensity of a sample is recorded and background corrected, the question arises as to which information can be obtained from it. We can summarize Eqs.(1) and (2),

$$\Delta I(q) = K \cdot P(q) \cdot S(q),$$

where we have lumped together all constant terms into . It is evident that there are three components to be considered. One is the constant , which consists of the particle contrast, volume, concentration etc. This constant is important to know when the molecular weight of the particles is investigated.

The other factors, P(q) and S(q), have their value in their angle dependence, only. The intensity units are of no concern. The form factor P(q) bears the shape and the internal density distribution of the particles. The structure factor S(q) carries the information about particle-particle interactions, such as inter-particle distances and degree of order to name just a few. When distances and shapes are to be determined, then the first question should address the range of distances, which can be observed.

5.4.1 The resolution

Owing to its close relationship to microscopy (see „Scattering and microscopy“ on page 10), SAXS is equally limited in resolving details of structure. In any optical experiment, objects of size D can be detected only in a limited range, starting from a smallest distance D_{min} and ending at a largest distance D_{max}. In microscopy as well as in SAXS these limits are established by the wavelength of the radiation and by the aperture of the lens, i.e., the range of scattering angles $q_{min} < q < q_{max}$ between which the scattering pattern (or the form factor) is sampled.

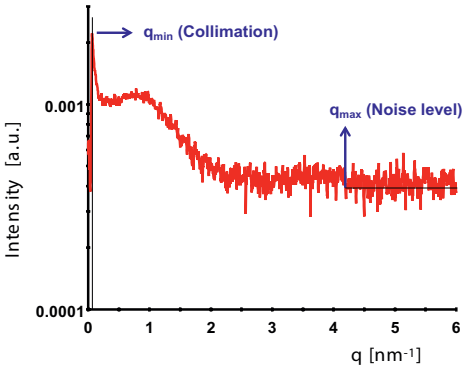

Fig. 5 - 24.

The two limits for the resolution of a scattering curve.

The lower limit q_{min} is due to the presence of the primary beam and is governed by the quality of the collimation system. The upper limit q_{max} is due to the fading of the signal into the noise level. Without going into mathematical details (see the Nyquist theorem[23] of the Fourier transformation), we just give the result that a scattering profile, which is measured between q_{min} and q_{max}, can be used to resolve particle features only between D_{min} and D_{max} ,

$$D_{min} \approx \frac{\pi}{q_{max}}, \qquad [nm]$$

$$D_{max} \approx \frac{\pi}{q_{min}}, \qquad [nm]$$

For SAXS the technological challenge is to reach a small q_{min} without disturbance of the signal by the much stronger direct beam. The quality of the collimation system and the alignment of the beam stop are the main ingredients which determine the accessible q_{min}. Therefore the quality of a SAXS device is usually specified in terms of q_{min} or D_{max} . Typical SAXS instruments have a resolution of about D_{max} = 30 - 50 nm.

Sometimes people specify the resolution by means of a largest "Bragg distance"

$$d_{Bragg} = \frac{2\pi}{q_{Peak}}, \qquad [nm]$$

where d_{Bragg} is the lattice spacing of a crystal plane whose reflection is hypothetically positioned at q_{Peak}. The discrepancy between d_{Bragg} and q_{Peak} is a factor of two. So, how come that a lattice distance two times larger than the resolution limit can be considered resolved? The answer is simple: It isn't. If a peak had its maximum at one end of a curve, then one could not even tell that it is a maximum. Not even its position would be determined. In order to call a peak resolved, it must lie within the curve. Thus a Bragg-peak position can never be used for a resolution specification, because $q_{min} < q_{Peak} < q_{max}$ must hold.

5.4.2 Radius of gyration

Any form factor P(q) can be approximated by a Gaussian curve at small angles. According to Guinier (1939), the curvature of this Gaussian is due to the overall size of the particles, so that

$$P(q) \approx a_0 \cdot e^{-\left(\frac{R_G^2 q^2}{3}\right)}.$$

The size parameter R_G is called the "radius of gyration". It is model independent. That means it contains no information about the shape or the internal structure of the particle. But if the structure of the particles could be assumed, then R_G could be used to calculate the particle dimensions. For example, if the particles are known to be spherical with an equal density everywhere inside (i.e., with a homogeneous density), then the average radius of such particles could be calculated from the radius of gyration by $R = \sqrt{(5/3R_G)}$. Other equations can be derived for any other particle shape.

The parameter a_0 is the extrapolated zero-angle intensity. In the equation above $a_0 = 1$, because P(0) = 1 by definition, but if ΔI(q) is used instead, then $a_0 = \Delta I(0)$, which can be used to determine the molecular weight (see 5.4.4 “Molecular weight”). In a so-called Guinier plot, the logarithm of the intensity is printed versus q^2,

$$ln[\Delta I_{(q)}] = ln[a_0] - \frac{R_G^2 q^2}{3}.$$

The parameters R_G and a_0 are determined by straight-line fitting from the slope $-(R^2_G/3)$ and from the intercept $1n(a_0)$ as shown in Fig. 5 - 25.

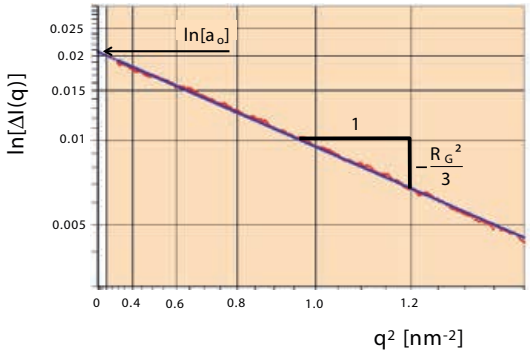

Fig. 5 - 25.

Guinier’s plot of a form factor in order to determine the particle’s radius of gyration R_G and the zero-angle intensity a_0.

Interestingly, almost the same radius of gyration can be obtained, even if line-smeared intensity data ΔJ(q) are used instead of ΔI(q). This is not quite unexpected since the exponent of a Gaussian function does not change upon integration. Still, the radii of gyrations from line-smeared data come out too large (by about 4 %) due to Guinier’s approximation that the form factor is equal to a Gaussian curve.

Note, that the obtained size parameter is the average of squares ($<R^2_G>$) and that only in sufficiently monodisperse cases the

linear size parameter can be obtained by taking the square root, $\langle R_G \rangle \approx \sqrt{\langle R^2_G \rangle}$. The monodispersity criterion is indicated in a Guinier plot, when the data points fall onto a straight line. If the sample is polydisperse (particularly when some particles are larger than the resolution limit), then the data points do not fall onto a straight line. In this case, the Guinier approximation fails and should not be applied. The only way out in such cases would be the calculation of the size distribution by inversion techniques (see 5.4.6 “Polydispersity analysis”).

At very small angles the data points suddenly drop below the fitted line (see Fig. 5 - 25.). This sudden intensity drop is caused by the beam stop. The edge at q_{min} indicates the resolution limit of the instrument. Thus, a Guinier plot is very useful for finding the resolution limit (q_{min}) of an experiment.

When cylindrical particles are considered, then the “radius of gyration of the cross-section” R_C can be extracted by using

$$q \cdot P(q) \cong a_0 \cdot e^{-\left(\frac{R_C^2 q^2}{2}\right)} \qquad [nm^{-1}].$$

This works even when the axial dimension is larger than the resolution limit, because the form factor is multiplied by q, which cancels the contribution of the axial dimension (assumed to be infinitely long). The radius R of a circular homogeneous cylinder can then be calculated by $R = \sqrt{2} R_C$. When ΔI(q) is used in absolute units instead of P(q), then a_0 is proportional to the molecular weight per unit length.

For lamellar particles a similar equation can be used

$$q^2 \cdot P(q) \cong a_0 \cdot e^{-\left(R_T^2 q^2\right)}, \qquad [nm^{-2}]$$

where R_T is the thickness radius of gyration. For a homogeneous plate the half thickness R theoretically equals $R = \sqrt{3}R_T$. When applied with absolute-intensity data, the parameter a_0 can be used to calculate the molecular weight per unit area.

5.4.3 Surface per volume

There are two general rules originating from Porod (1951) that apply to scattering profiles. The first rule states that the scattering profile of any particle system decays at large scattering angles with K_P/q^4, where the constant K_P is proportional to the surface per sample volume. The other rule is that the second moment of any scattering profile is a universal constant, called “the invariant”,

$$Q_P = \int_0^\infty q^2 \Delta I(q) dq \qquad [a.u./nm^3].$$

The invariant contains instrumental factors which are not easy to obtain, such as the primary beam intensity and the illuminated sample volume. But the same factors also appear in the constant K_P. Because the invariant is a theoretically well-defined constant, it can be used in a quotient to cancel the unknown instrumental factors. This is straight forward, because both parameters, Q_P and K_P, are calculated from the same data set. In this way the surface per volume can be calculated

$$\frac{S}{V} = 1000 \cdot \pi \cdot \frac{K_P}{Q_P} \cdot \varphi(1-\varphi) \qquad [m^2/cm^3],$$

where φ is the volume fraction of the particles, which must be determined by independent means, such as Helium-Pycnometry (for porous solids) or concentration protocols (for dispersions and emulsions).

This method can also be applied to dense particle systems, because inter-particle interferences have no effect at large angles (i.e., S(q) ≈ 1). The accuracy of the resulting surface-per-volume values is not very high, though. That is caused by two facts.

1. The constant K_P is determined from the final slope of ΔI(q), which is close to the background level and usually very noisy.

2. The invariant Q_P must be calculated by extrapolating ΔI(q) towards zero and infinitely large scattering angles, i.e., into regions where no experimental data are available. The first extrapolation can be done by applying Guinier's approximation and the second extrapolation can be done by applying Porod's q^{-4} dependence.

Modified equations apply approximately, when line-collimation experiments are used

$$\frac{S}{V} \approx 4000 \cdot \frac{K_L}{Q_L} \cdot \varphi(1-\varphi) \qquad [m^2/cm^3],$$

where K_L is calculated by fitting $\Delta J(q) \approx K_L/q^4 + B$, and the invariant Q_L is the first moment of the smeared intensity,

$$Q_L = \int_0^\infty q \Delta J(q) dq \qquad [a.u./nm^3].$$

These last modified equations hold strictly only for the assumption of an infinitely long primary-beam profile.

5.4.4 Molecular weight

SAXS can also be used to determine the mean molecular weight [g/mol] of particles[25], because the scattered intensity is proportional

to the squared particle volume V_1. If we knew the density d_1 of the dispersed particles as well, then we could calculate the molecular weight from the scattered intensity. But let us first convert the ingredients of Eq.(1) into a form amenable to experimenters. Equations (1) and (2) can be combined

$$\Delta I(q) = I_0 \cdot N \cdot V_1^2 \cdot (\Delta\rho)^2 \cdot P(q) \cdot S(q). \qquad [a.u.]$$

We express the total volume of illuminated particles $NV_1 = (c \cdot V_S)/d_1$ in terms of concentration c [g/cm^3], density of the particle material d_1 [cm^3/g] and illuminated sample volume V_S [cm^3]. Likewise, the particle volume $V_1 = M/(N_A \cdot d_1)$ can be converted into molar particle mass M [g/mol], where $N_A = 6.0221367 \cdot 10^{23}$/mol is Avogadro's number. Substitution renders the contrast $\Delta Z = \Delta\rho/(N_A d_1)$ in units of mol electrons per gram

$$\Delta I(q) = I_0 \cdot V_S \cdot N_A \cdot c \cdot M \cdot \left(\frac{\Delta\rho}{N_A d_1}\right)^2 \cdot P(q) \cdot S(q). \qquad [a.u.]$$

We can write the contrast as a difference of mol electrons per gram $\Delta Z = Z_1 - \overline{v}_1\rho_2$, where Z_1 is the mol of electrons per gram particle material [mol/g], $\overline{v}_1 = 1/d^1$ is the specific volume of the particle [cm^3/g] and ρ_2 is the electron density of the solvent in [mol/cm^3]. We also have to make the equation independent of the primary-beam flux density i_0 [a.u./cm^2] and the illuminated sample volume V_S [cm^3]. The constant factors are put together into $K_0 = I_0 \cdot N_A/i_0$ [cm^2/mol], so that the intensity can finally be written in terms of concentration, contrast and molecular weight of the particles.

$$(4) \qquad \Delta I_{abs}(q) = \frac{\Delta I(q)}{i_0 \cdot V_S} = K_0 \cdot c \cdot M \cdot (\Delta Z)^2 \cdot P(q) \cdot S(q), \qquad [cm^{-1}]$$

Note that the intensity is now in absolute units (see 5.3.3 “Intensities on absolute scale”).

The contrast $\Delta Z = Z_1 - \overline{v}_1\rho_2$ must be determined independently with a density meter capable of measuring high-precision density values of solvent (d_2) and dispersion (d). Good approximations for $\overline{v}_1$ can be obtained by calculating apparent values $\overline{v_{app}} = (c-d-d_2)/(cd_2)$ from a series of concentrations c.
The electron density of the solvent ρ_2 can be calculated from the knowledge of its chemistry. If one solvent molecule of molecular weight m_2 has e_2 electrons, then its electron density is $\rho_2 = (e_2 \cdot d_2)/m_2$. The number of mol electrons per gram Z_1 can be calculated in the same way, $Z_1 = e_1/m_1$.
If the form factor and the structure factor are known, say, by fitting the data $\Delta I(q)$, then the molecular weight could be determined at any q-value using

$$M = \frac{\Delta I(q)}{K_0 \cdot c \cdot (\Delta Z)^2 \cdot P(q) \cdot S(q)}. \qquad [g/mol]$$

If a correct model for $P(q) \cdot S(q)$ cannot be found, then people try to extrapolate $\Delta I(q)$ towards zero scattering angle, so that $P(0) = 1$. In order to apply $S(q) \approx 1$ one also extrapolates towards negligible concentration. A series of scattering curves are measured at different concentrations. These are extrapolated[24] at every q-value, as is commonly done in light scattering with a so-called Zimm plot.

5.4.5 Particle structure

Every particle produces a form factor that is characteristic to its structure. The slope of the form factor at small angles is primarily determined by the overall size and the final slope at large angles bears the information of the surface. The information about the shape and the internal density distribution lies in the oscillating part in the middle section of the form factor.

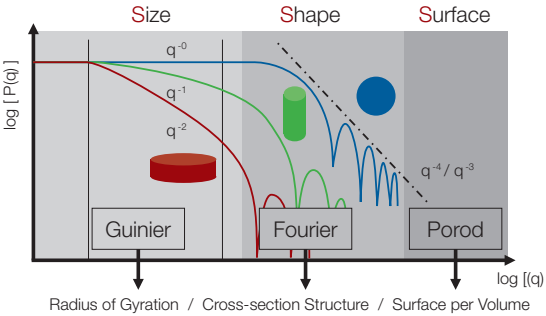

Fig. 5 - 26.

The information domains of a particle form factor.

A rough classification into globular, cylindrical and lamellar shape (with axial ratios bigger than 5) can be quickly done by investigating the power law of the form factor at small angles (see Fig. 5 - 26.). In a double logarithmic plot an initial slope of 0, -1 or -2 indicates globular, cylindrical or lamellar shape, respectively. If the slope is steeper than that (e.g., -3 or -4) then the particles are larger than the resolution limit and the Porod region is the only part of the form factor that can be observed.

The oscillating part of the form factor can be profitably investigated by transforming it into “real space”, i.e. the calculation of p(r) from an experimental P(q) via

$$P(q) = 4\pi \int_0^\infty (p) r \frac{sin(qr)}{qr} dr.$$

The applied method is basically a Fourier-transformation and the resulting curve, p(r) , is a so-called “pair-distance distribution function” (PDDF). This is a histogram of distances which can be found inside the particle. Details of how these PDDFs are calculated can be found in the original literature.[22] It is not within the scope of this document to present these details. Instead, let us discuss the features of a PDDF which give indications about the particle structure. The shape of a particle can be quickly classified into spherical (or

globular), prolate (or cylindrical) and oblate (or lamellar) symmetry by identifying some key features in the PDDF as shown in Fig. 5 - 27.

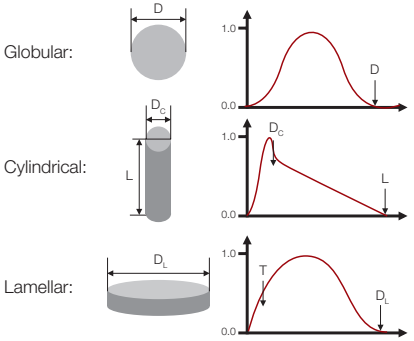

Fig. 5 - 27.

The key features of the PDDF, which are indicative for the particle shape.

Globular particles can be identified from the bell shaped, almost symmetrical peak. Cylinder particles are identified by a small overshoot and a linear tail in the PDDF. The PDDFs of lamellar particles are not bell shaped at small r-values. They have a resemblance to the globular PDDF, but the curvature at small r-values is different (see Fig. 5 - 27.). All PDDFs decay to zero at some distance r, which indicates the largest distance that can be found inside the particle.

Inhomogeneous (or core-shell) particles are also quickly discovered, because the PDDF is a histogram of distances which is weighted by the contrast values ($\Delta\rho$) that are connected by each distance. So, all distances that cross the border from positive to negative $\Delta\rho$-values count negative. This causes a dip in the PDDF, which can even go to negative (see Fig. 5 - 28.), when the contrast of one region is smaller than that of the matrix material. The contrast of the matrix material counts zero and all distances, which connect matrix material with particle material do not count at all.

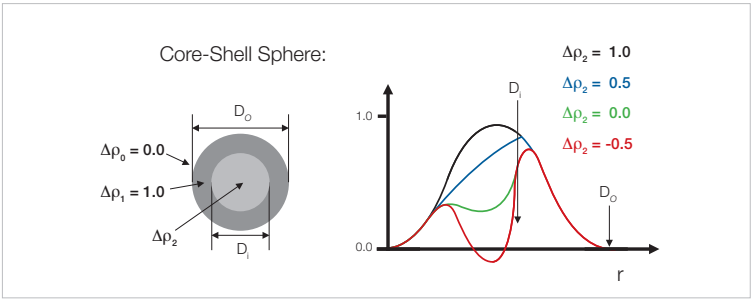

Fig. 5 - 28.

The PDDFs of core-shell particles.

It is comparatively easy to recognize the PDDFs of aggregates, i.e., of particles that stick together. They show a second peak, too. But in contrast to the second peak in the PDDF of a core-shell particle, it is smaller than the first peak (see Fig. 5 - 29.).

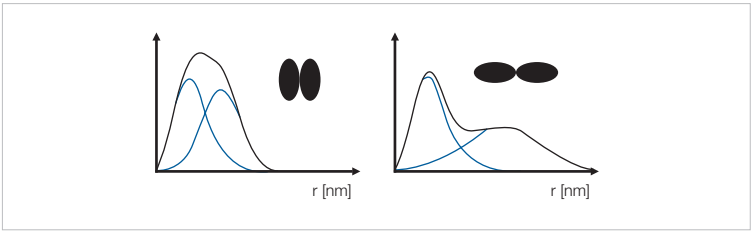

Fig. 5 - 29.

The aggregate of two subunits make a PDDF which can be recognized by a second peak.

Particles of arbitrary shape produce PDDFs that cannot be analyzed without additional information. In general, it must be noted that any PDDF, as well as the scattering function is ambiguous, when polydispersity or polymorphism are taking part. Any shape can be generated by a “smart-enough” distribution of polydisperse spheres or other shapes. So, microscopic techniques should always be used to complement the proof of structure.

When particles are centro-symmetric (i.e., spherical, cylindrical or lamellar), then their PDDFs can be transformed (deconvoluted) [28],[29] into the corresponding radial density profiles. For all other particle symmetries, model calculations[30]-[34] must be performed and compared to the experimental PDDF (or form factor) in order

to refine a structure model. This can also be attempted directly by means of fitting routines[32]-[34] which can cope with the challenges of local minima in the search for the best-fitting structure.

5.4.6 Polydispersity analysis

The particle shape concluded from SAXS experiments is always ambiguous, if no additional information about the sample is available from some other technique, such as electron microscopy. The ambiguity lies in the fact that the shape of a PDDF (as well as the shape of a form factor) is the average of ALL illuminated particles in the sample. And these can be many! The PDDF is therefore the sum of contributions from

1. identical particles (in **monodisperse** samples),

2. particles of the same general shape but different size (in **polydisperse** samples)

or

3. particles of totally different shapes and sizes (in **polymorphous** samples).

Extracting the single components from the experimental form factor or the PDDF is known as polydispersity analysis. It can be done with the same basic concept shown previously in the synthesis (see Fig. 3 - 12.). It is important to know, however, that it is possible to split up the experimental PDDF (or form factor) into a unanimous distribution of sizes, only when the shape of the particles is established.
If a sample contains two different but known shapes, then the relative volume fractions of the two particle species can be quantitatively determined by calculating the best fitting coefficients (a and b) of the following equation,

$$P_{sample} = a^2 \cdot P_{shape1} + b^2 \cdot P_{shape2},$$

where P_{shape1} and P_{shape2} are the theoretical PDDFs or form factors of the respective shape or size component. The parameters a and b are the respective volume fractions of each component.
Once the shape is established, the size distribution of one parameter, such as the particle radius, can be calculated by an inversion of

$$P_{exp}(q) = \int_0^\infty D_I(R) P(q,R) dr.$$

P(q, R) is the theoretical form factor of the assumed shape and D_1 is the intensity-weighted size distribution. Volume and number distributions can also be obtained by using $D_V = D_I/V_1$ and $D_N = D_I/V_1^2$, respectively. Once the size distribution is calculated, the mean particle size $\langle R \rangle_I$ and the mean distribution width $\sigma 1(R)$ can be calculated therefrom,

$$\langle R \rangle_I = \int_0^\infty R D_I(R) dR, \qquad \sigma_I(R) = \sqrt{\langle R^2 \rangle_I - \langle R \rangle_I^2} \qquad [nm].$$

For volume and number weighted averages, the corresponding distributions must be used instead of D_1. Here we take it that the distributions are all normalized to unit area.

5.4.7 Model calculations

When the structure of a particle is known to consist of a couple of known subunits, then model calculations are needed to determine the relative positions and orientations of the subunits. The determination consists of repeated calculations of theoretical PDDFs (or

form factors). Comparisons with the experimental curves then help to decide which changes are needed to improve the fit. The subunit configuration that fits best is taken as the refined structure model.

Of course, structure refinements only make sense, when it is established that the experimental PDDFs or form factors are from monodisperse samples. The presence of any diversity in size or shape is detrimental to a structure determination.

Computer programs that can be used to model form factors and PDDFs are abundant and available.[30]-[34]

5.4.8 Particle interaction

When determining the single-particle structure, most of the time the structure factor *S(q)* cannot be neglected. For this you would have to dilute your sample and this is not always practicable, because

1. a minimum concentration is required to get sufficient particle scattering above the background level (particularly with low-contrast samples such as proteins in solution).

2. the particle structure can change with the concentration (e.g., surfactants in solution) and this fact might even be the reason for the investigation.

Interparticle forces are responsible for the development of a structure factor. The interaction strength depends on the concentration of the particles and on the force they exert on each other. Known force classes or interaction types are briefly listed here.

1. **Hard-sphere interaction:** The particles can move freely but cannot penetrate each other. It is described by a hard-sphere radius and a concentration.

2. **Coulomb interaction:** Particles that carry electrical charges can move freely unless their electrical fields start to penetrate and repel each other. It is described by an effective hard-sphere radius, a concentration, a surface charge and an ionic strength of the solvent (which leads to a layer of counter ions that shield off the electrical fields of neighboring particles).

3. **Van-der-Waals interaction:** Refers to those forces which arise from the polarization of molecules into dipoles. It is a property that all molecules have. Condensation and aggregation of particles are caused by it, because it makes particles attract each other, once they have reached a minimum distance. The parameters are an effective hard-sphere radius, a concentration and two exponents that describe a short-ranged attraction and a long-ranged repelling distance. The two exponents inherently form a potential minimum which defines an equilibrium inter-particle distance. The deeper the potential minimum, the more stable is the inter-particle distance.

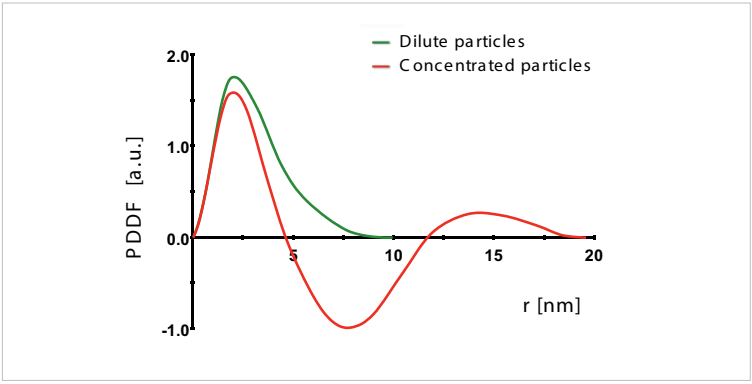

Fig. 5 - 30.

The PDDF of (red) a concentrated particle system shows a negative part with a minimum approximately at the largest dimension of the particle (D = 10 nm). Due to a shell of next-neighboring particles a second peak appears around r = 14 nm. The same particle system, but diluted, gives the green PDDF.

The first indication of interparticle interference is, when the scattering curve bends down at small q-values (see Fig. 3 - 8.). The

corresponding PDDF goes negative and shows a second maximum at larger distances (see Fig. 5 - 30.). The negative dip originates from the excluded volume caused by the presence of one particle which prevents other particles from entering the same volume (hard-sphere effect). The electron density in the excluded volume is therefore smaller than the bulk electron density (which is the zero line in the PDDF).
The second peak at larger distances is caused by a “shell” of next neighbors, which increases the density above the bulk level due to the locally increased particle concentration. This alternating arrangement of particle densities is commonly known as short-range order and is typical for the liquid-phase state.

At larger concentrations or stronger interaction forces the particles can rearrange into a long-range order, i.e., they develop a crystallinity, which is typical for a solid-phase state. In this case the PDDF oscillates up to large r-values with a periodicity of the unit-cell dimension. The corresponding scattering curve then shows Bragg peaks for every periodic component in the PDDF. The spacing of the peaks relative to each other tells something about the symmetry of the crystal system. The relative peak intensities reflect the form factor of the unit cell’s ingredients, because of the product of structure and form factor (see Fig. 5 - 31.).

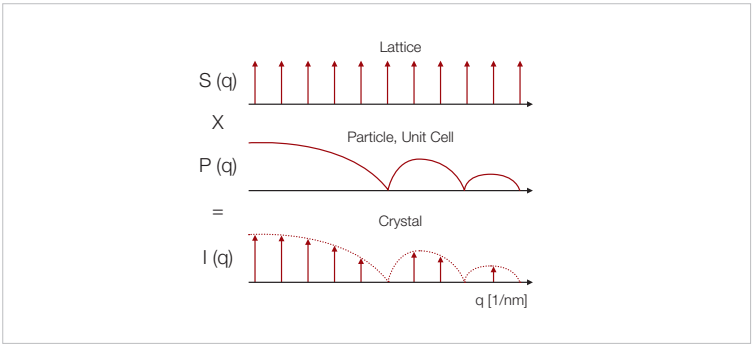

Fig. 5 - 31.

The scattering curve of a crystal I(q) is the product of the structure (or lattice) factor S(q) with the form factor P(q) of the particles (or atoms) in the unit cell. When lattice peak and form-factor minimum collide, then a so-called systematic extinction follows and the peak cannot be observed.

Other factors that influence the peak intensities are

1. the degree of order of the "particles", which leads to a decay of peak intensities with increasing scattering angle (the better the order, the smaller the decay and the more peaks can be observed at large angles) and
2. the spatial extent of a crystalline domain, which is reflected in the peak width (the larger the domain, the smaller the peak width).

In many practical applications it is desirable to eliminate the structure factor which obstructs the access to the single-particle structure. The old-fashioned way was to cut away data points at very small angles and interpret the particle structure from the scattering profile at larger angles. A much better method[27] is to fit a theoretical S(q) simultaneously with the PDDF. In this way the inter-particle terms are taken into account by fitting an effective S(q) and the single-particle terms are represented by the PDDF with only little disturbances from the S(q). In addition, the fitted S(q)-parameters can be used to retrieve interparticle parameters.

5.4.9 Degree of orientation

Particles of non-spherical shapes can have a preferred orientation due to applied shear or strain. The azimuthal profiles of randomly oriented samples (or with spherical particles) have a constant intensity along a circular path centered at the primary beam position. As soon as some preferred orientation is introduced into the sample (e.g. in block co-polymer melts) the intensity profile starts to oscillate or becomes peaked at certain azimuth angles. It is clear that the amplitudes of these oscillations are useful to quantify the degree of orientation. Also the angle of preferred orientation is of interest. There are two approaches commonly in use.

1. **Herman's orientation parameter** P_2 is a frequently used parameter to define the angle of orientation. It is defined by

$$P_2 = \frac{3\langle cos^2\phi\rangle - 1}{2}, \quad \text{where} \quad \langle cos^2\phi\rangle = \left(\int_0^{\pi} cos^2\phi \cdot \Delta I(\phi) sin\phi d\phi\right) / \left(\int_0^{\pi} \Delta I(\phi) sin\phi d\phi\right).$$

If P_2 = 1, then the intensity is perfectly peaked towards ϕ = 0°, if P_2 = -1/2, then it is perfectly peaked towards ϕ = 90° (anti-parallel). Confusion arises though, when P_2 = 0. Because this can mean that the intensity profile is either a constant (no orientation at all) or perfectly peaked towards the "magic angle" of ϕ = 54.7356°. This mix-up between degree and angle of orientation makes this parameter practically useless for SAXS applications.

2. **Cinader & Burghardt**[35] proposed to characterize anisotropy in SAXS patterns by an anisotropy tensor

$$S = \begin{bmatrix} S_{11} & S_{12} \\ S_{12} & S_{22} \end{bmatrix} = \begin{bmatrix} \langle cos^2\phi\rangle & \langle cos\phi sin\phi\rangle \\ \langle cos\phi sin\phi\rangle & \langle cos^2\phi\rangle \end{bmatrix}, \quad \text{where} \quad \langle z\rangle = \left(\int_0^{\pi} z\Delta I(\phi) d\phi\right) / \left(\int_0^{\pi} \Delta I(\phi) d\phi\right).$$

ϕ increases anti-clockwise, starting from 3 o'clock.

The degree of orientation is then defined by $\Delta S = \sqrt{(S_{11} - S_{22})^2 + 4S_{12}^2}$

and the mean orientation angle is calculated by $\chi = \frac{1}{2} atan[\frac{2S_{12}}{S_{11} - S_{22}}]$.

Possible values of ΔS lie between 0 (no orientation) and 1 (perfect orientation) and there is no ambiguity as in the case of Herman's orientation parameter.

It is also worth mentioning that Cinader & Burghardt's approach, as shown above, is sensitive towards a two-fold symmetry (C2). For example, a clover-leaf shaped intensity pattern, having a four-fold symmetry (C4), will give a zero degree of orientation (ΔS = 0), because it is not a two-fold symmetry. But the algorithm is easily extended to a 2n-fold symmetry by substituting cosϕ and sinϕ by cos(nϕ) and sin(nϕ), respectively. In the case of a clover-leaf pattern n would be 2.

5.4.10 Degree of crystallinity

The degree of crystallinity (DOC) is used to characterize materials which can exist in both modifications, amorphous (DOC=0) and crystalline (DOC=1). It tells us how much of the sample volume is in the crystalline state. It is, however, a relative measure, because it can only be determined, if an amorphous reference sample is available. Please note, that amorphous not necessarily means “no crystallinity at all”, but rather that it contains either no crystallinity or the “wrong” crystallinity. Thus, also the amorphous reference sample can have Bragg reflections in its scattering curve.

The DOC is determined by making two scattering experiments. One is the acquisition of the reference sample [$\Delta I_{amorphous}(q)$] and the other one acquires intensities of the sample under investigation [$\Delta I_{sample}(q)$]. The DOC is then calculated via

$$DOC = \left(\int_{q_{min}}^{q_{max}} q^2 [\Delta I_{sample}(q) - _{amorphous}(q)] dq \right) / \left(\int_{q_{min}}^{q_{max}} q^2 \Delta I_{sample}(q) dq \right).$$

The background must be carefully subtracted before the DOC is calculated, because any residual baseline will make the integrands rise quickly due to the multiplication with q^2.

If an amorphous sample is not available, then an assumed smooth background curve must be used, which makes the results less accurate. One good way of determining the background curve was devised by Steenstrup[36].
Finally, we have to mention that the determination of a DOC is a common quest in XRD (WAXS) but it is a relatively rare sought-after value in SAXS applications due to the enhanced difficulty of determining the background.

➤ 5.5. Data interpretation in reflection mode

Data from surface-scattering experiments need special treatment and interpretation. This also requires that we have to reconsider the previously simplified definition of the momentum transfer.

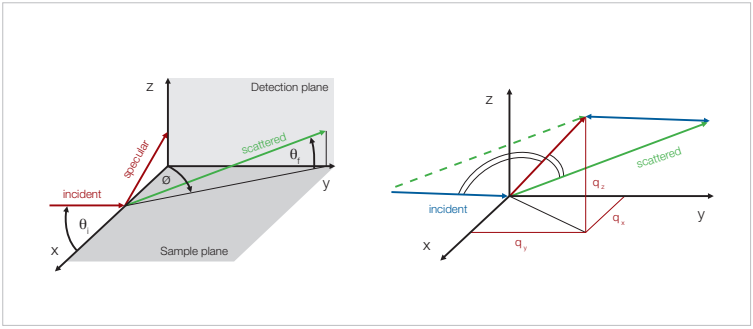

Fig. 5 - 32.

Every point in the detection plane can be attributed to a scattering vector, which is the difference of the two directions: scattered minus incident direction.

If we define the scattering geometry as shown in Fig. 5 - 32., then the scattering vector is defined by

$$\vec{q} = \begin{bmatrix} q_x \\ q_y \\ q_z \end{bmatrix} = \frac{2\pi}{\lambda} \begin{bmatrix} cos\theta_f cos\phi - cos\theta_i \\ cos\theta_f sin\phi \\ sin\theta_f + sin\theta_i \end{bmatrix}, \qquad [1/nm].$$

Until now we were confronted with the z-component (q_z) only and we have called it q for short. In XRR experiments the detection angle is strictly the same as the angle of incidence ($\theta_f = \theta_i$ and $s = \phi$). It follows that $q_z = q$ and $q_x = q_y = 0$. In GI-SAXS experiments scans along q_y and q_z are extensively used.

5.5.1 XRR Data

X-ray reflectivity data R(q) are the ratio of reflected ($\Delta I_{spec}(q)$) versus incident (I_0) beam intensities. The reflectivity of a perfectly flat but rough surface is

$$R(q) = \frac{\Delta I_{spec}(q)}{I_0} = \left| \frac{q_z - \sqrt{q_z^2 - q_c^2 - iB}}{q_z - \sqrt{q_z^2 - q_c^2 - iB}} \right|^2 e^{-\left(\frac{\sigma^2 q_z^2}{2}\right)}.$$

The critical momentum transfer q_c, the absorption coefficient B and the root-mean-square (RMS) roughness σ can be regarded as fitting parameters. q_c and B are used to determine the density or the chemical composition of the surface layer. The roughness parameter is mainly used for compensation purposes. Surfaces with large roughness are not suited for XRR experiments, because of the exponential damping of the reflected beam leading to a small signal strength. The signal is diffusely scattered and GISAXS would be the better choice in such situations.

The most prominent application of XRR is the characterization of multilayered surfaces. Already one single layer of another material (e.g., an oxide layer) on a flat substrate leads to Kiessig fringes in the reflectivity curves, which can be used to determine the layer thickness.

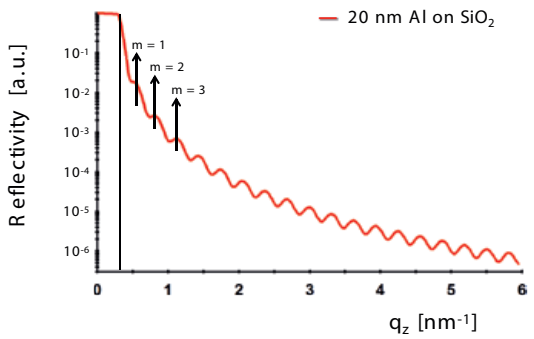

Fig. 5 - 33.

The XRR curve of a 20 nm thick layer of Al on a quartz substrate (no roughness). The dashed vertical line indicates the critical angle of the Al surface.

When you measure the peak-maximum positions q_m and plot them versus the fringe-order number m (i.e., $y = q_m^2$ versus $x = m^2$), you can get the critical momentum transfer q_c and the layer thickness by straight-line fitting of

$$y = q_c^2 + \left(\frac{2\pi}{d}\right)^2 \cdot x, \qquad [1/nm^2].$$

From the intercept you can determine the electron density ρ_1 of the surface layer by

$$\rho_1 = (q_c/0.292)^2, \qquad [mol/cm^3].$$

If the surface layer is rough, then the fringes are less visible and more sophisticated fitting procedures are required to determine the layer thickness. Strong surface roughness can make XRR experiments prohibitive.

XRR data always need cleaning from scattering contributions. You can separate the reflected intensity (ΔI_{spec}) from the diffusely scattered intensity (ΔI_{diff}) by subtracting a curve recorded slightly off-specular, i.e., at $\theta_f = \theta_i + \delta\theta$, where $\delta\theta$ is an offset value slightly larger than the width of the direct beam. This subtracts off a baseline curve, which contains diffuse scattering and dark-counts of the detector.

Surface roughness can also be regarded as a gradual transition of the density from one layer to the next. In this way any roughness can be modeled by a hypothetical stack of thin (and smooth) layers, which constitutes an effective-density profile. In this context and under a few assumed simplifications, it can be quite useful to use inverse Fourier transform methods to extract density profiles in a model-free way from XRR curves (for details see Gibaud[13]).

5.5.2 GI-SAXS Data

GI-SAXS probes surface structures. This means that there have to be particles or other inhomogeneities on the surface that scatter diffusely the incoming beam. Because of the small entrance angle

a large surface area is investigated at the same time in one experiment. For example a 0.3 mm wide beam at a typical entrance angle of 0.2 degrees would have a footprint on the sample of 90 mm length. If we allow half of the beam to pass over the sample without touching, then still a sample length of 45 mm length is screened at once in a typical GI-SAXS experiment.

The 2D data $\Delta I_{diff}(q_y, q_z)$ show features of the surface structures. In case of ordered structures the patterns give immediate information of the general aligment of the structures relative to the surface. As shown in the schematic (see Fig. 5 - 34.) periodicities along the y and z-direction give rise to Bragg peaks in the q_y and q_z-direction, respectively.

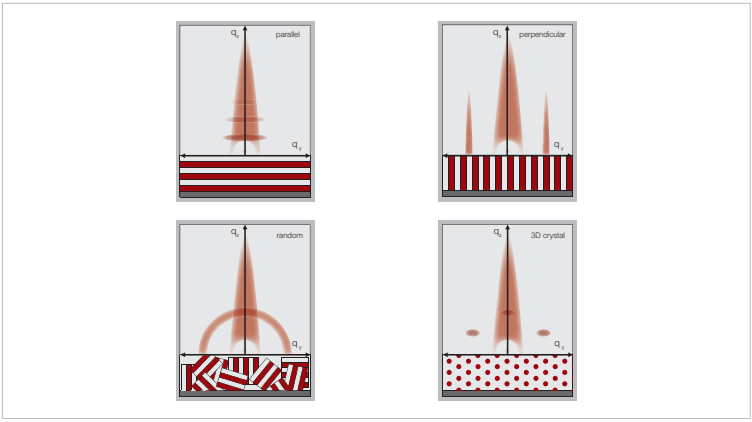

Fig. 5 - 34.

Features of GI-SAXS patterns (red) of different periodic thin-film structures (green). The central yellow streak along the q_z-axis is due to the surface roughness. The q_y-axis is drawn at the approximate height of the specular reflection (not shown).

Nonperiodic structures will produce scattering curves rather than Bragg peaks. Two fundamentally different ways of structure interpretation exist.

1. **The roughness-correlation approach** (W. Weber and V. Holy[16]-[18]): The scattering curves are calculated from the surface

roughness, which is described by employing a spatial height-height correlation function, $C(r) = \sigma^2 \cdot \exp[-(r/R)^{2h}]$, where σ is the RMS roughness amplitude, R is a lateral length at which the surface begins to "look" rough and h is the Hurst parameter specifying, on a scale between 0 and 1, the jaggedness of the roughness. Alternatively, particularly for liquid surfaces and for $h < 0.5$, it is advisable to use other model functions (see e.g. the K-correlation function described by Tolan[14]) that explain the scattering curves of liquid surfaces much better.

2. **The particle-system approach** (R. Lazzary[19]): The scattering curves are calculated from particles of assumed shapes, sizes, heights, densities and distances in between. The program IsGISAXS is in wide-spread use, because it is freely available for the academic community.

The accompanying reflection signal is tuned out, either by an extended beam stop or by including the specular reflectivity signal into the fitting theory.

Identical equations, as applied to ordinary (transmission-mode) SAXS data, can be used here as well. Quick interpretations are possible, when 1D profiles in the q_y and q_z directions are extracted from the 2D GI-SAXS pattern. These two profiles can be evaluated by applying the previously mentioned Guinier, Fourier and Porod evaluations (see chapter 5.4).

$$I(q_y) = K_y \cdot P(q_y) \cdot S(q_y), \qquad [a.u.]$$

$$I(q_z) = K_z \cdot P(q_z) \cdot T(q_z - q_{z0}) \qquad [a.u.].$$

Here, the scaling factors K_y and K_z bear the contrast information and the form factors $P(q_y)$ and $P(q_z)$ carry the averaged particle shape/

size and height information, respectively, as in ordinary SAXS. The structure factor is for two dimensional liquids as opposed to the three-dimensional liquids in SAXS.

The vertical profiles $I(q_z)$, however, contain the Fresnel transmission function $T(q_z - q_{z0})$, which is responsible for the Yoneda peak at q_{z0}. Normally, they do not employ a structure factor, unless there are particle-particle correlations (e.g. periodicities) normal to the surface. If such correlations exist, as for example in a multilayer with the roughness contours of every layer boundary running mostly parallel, then a structure factor (i.e., Kiessig fringes and Bragg peaks) can be observed in the vertical profiles as well [see Fig. 5 - 35.(b)].

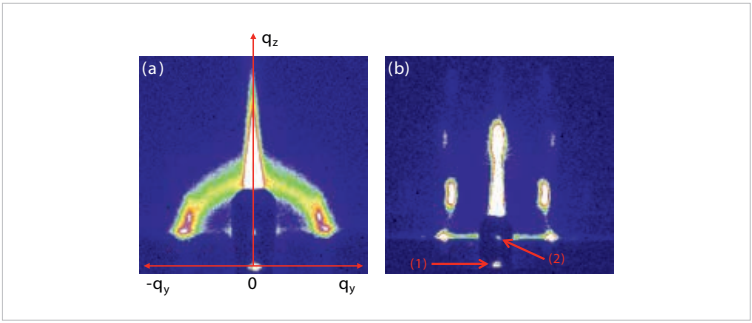

Fig. 5 - 35.

The GI-SAXS patterns of crystalline thin-film samples. The direct beam (1) and the specular beam (2) are attenuated by the beam stop. (a) Mixture of randomly oriented crystalline domains (half circle) and two preferred orientations (two red spots). The strong surface roughness leads to broad scattering along q_z. (b) A 3D single-crystal film. The vertical correlations between the crystal planes give rise to additional higher order Bragg peaks in q_z.

The interpretation of these features is analogous to the previously explained interpretations, with the additional complication of multiple scattering effects (interference of scattered with reflected and refracted beams) which are lumped together into the transmission function $T(q_z - q_{z0})$ in the equation above.

➤ 5.6. Summary

As a conclusion of this part of the booklet we should summarize the parameters that affect the scattered intensity and, thus, have an influence on the SAXS-signal quality.

1. **Size:** The intensity of the scattering signal goes with the sixth power of the particle size. The larger the particles are, the more intensity will be detected from them. However, there is an upper limit to this statement. Particles which are bigger than the spatial resolution limit of the setup (see „The resolution“ on page 61), will scatter to inaccessibly small angles and, thus, become invisible. But, generally, large particles will overshadow the signal of the smaller ones.
2. **Volume:** The sample volume increases the intensity linearly. Twice the illuminated sample volume will give twice the intensity and √2-times the signal quality. Care must be taken that the sample volume is maximized without exceeding the optimum sample thickness (see „Absorption“ on page 15).

3. **Contrast:** The electron-density difference between particles and matrix material (e.g., the solvent) increases the intensity quadratically (see „Contrast“ on page 52). Given the choice, one should always opt for a low-density solvent to maximize the contrast of the dispersed particles. On the other hand, one can make bothersome particles invisible by matching their contrast and facilitate the analysis of mixtures.

4. **Sample-to-detector distance:** Because the sample scatters into all directions, the scattered intensity is diluted over the surface of an ever increasing sphere, the surface of which increases with the squared radius R. Therefore short instruments (with a small sample-to-detector distance R) have a much higher efficiency than long instruments. The objection, that longer instruments have a higher resolution, is not always true, because the divergences of beam and optics determine the resolution. And these do not improve, if only the sample-to-detector distance is increased.

5. **Resolution:** Whenever the divergence of the beam is reduced to resolve large particles, the intensity of the setup suffers. USAXS instruments (e.g., Bonse-Hart systems) with really a whopping resolution in the micrometer range use crystal optics to reduce the divergence so much, that even the primary beam can no longer harm the detector. It is clear that the samples then must have sufficient contrast and size to produce a scattered intensity comparable to the primary-beam intensity. Otherwise there will not be enough photons reaching the detector.

6. **Collimation:** Every collimation has its function. The function of point collimation is to resolve orientation effects, not to improve the signal quality or resolution. Similarly, the function of line collimation is to improve signal quality and resolution, not to investigate orientation effects.

6. Scientific and industrial applications

➤ 6.1. Introduction

More than 100 years have passed since the discovery of X-rays. The rapid technological developments of X-ray sources, optics, computing power and software programs have revolutionized many experimental techniques, which have evolved X-ray methods and their increasingly dominant role in the characterization of materials. Many of these methods have become routine practice among scientists and researchers who study materials at atomic, molecular and super-molecular structure levels and the material's structure relationship to physical, chemical and biological properties.

Small-angle X-ray scattering (SAXS) is a fundamental method for structure analysis of condensed matter, and has emerged as an essential tool used to unravel structure details with characteristic dimensions at length scales of up to 100 nm and beyond. It is used at all fronts in material science for development purposes. The SAXS method yields information on the sizes or shapes of particles and also on the internal structure of disordered and partially ordered systems. The corresponding method to analyse structures spread over planar surfaces is grazing-incidence SAXS. This is a relatively new method but the interest in it is ever increasing.

The applications cover various fields, from metal alloys to synthetic polymers in solution and as bulk material, biological macromolecules, emulsions, porous materials, nano-particles, etc. In the 1960s, the method became increasingly important in the study of biological macromolecules in solution because it allowed for the first time to get low-resolution structural information on the overall shape without the need to grow crystals. Moreover, SAXS also makes it possible to investigate in real time[37]-[41] intermolecular interactions such as self-assembly and large-scale conformation

changes, on which biological functionality often relies. The random orientation of particles in solution leads to an averaged scattering pattern, so that only a one-dimensional information about a three-dimensional structure can be obtained. The main difficulty and simultaneously the main challenge of SAXS as a structural method is to extract information about the three-dimensional structure of the object from these one-dimensional experimental data. In the past, only overall particle parameters (e.g., mean radius of gyration, particle symmetry, surface per volume) of the macromolecules were directly determined from the experimental data, whereas the analysis in terms of three-dimensional models was limited to simple geometrical bodies (e.g., spherical, cylindrical, lamellar).

For inorganic and especially polymeric systems, integral parameters extracted from SAXS are usually sufficient to answer most of the structural questions. Electron microscopy (EM) was, and still is, often used as a guide to build consensus models. The 1990s brought another class of SAXS data analysis methods, allowing ab initio shape and domain structure determinations[32]-[34] and detailed modeling of macromolecular complexes using rigid body refinement.

The rationale behind new developments in modern materials science is to tailor a material (by varying the chemical composition, constituent phases and microstructures) in order to obtain a desired set of properties suitable for a given application. A key driver in the development of modern materials of today has been the ability to control their structure and functional properties and its relationship to the potential applications in the emerging fields of nano-materials. The self-assembled and hierarchical structures and the functions offered by these self-assemblies, such as micelles, liquid crystals, emulsions, liposomes, and solid-gels, consisting of amphiphilic organic polymers, are utilized in a wide variety of industrial fields. In addition, not only self-assemblies of organic amphiphiles, but also nano-structured inorganic materials, such as composite TiO_2 particles and mesoporous silicas and modified biological substances (e.g., recombinant and purified proteins) are in great demands.

The properties of functional materials are strongly linked to their size, shape, internal structure and interaction potential. To understand and develop functionalized materials, one requires advanced computer programs to evaluate scattering data. Data evaluation forms an important and integral part of SAXS experiments and is required to understand material properties in detail. In dense systems the scattered intensity is a combination of single-particle scattering (form factor) and inter-particle scattering (structure factor). Available standard programs usually assume diluted systems, and neglect the particle interaction. In many applications, it is undesirable or even impossible to dilute a sample. One of the most recent developments in data-evaluation programs now allows the interpretation of such data, the Generalized Indirect Fourier Transform method.[27] It facilitates the determination of the form factor and the structure factor simultaneously from experimental data with a minimum of a priori information.

It is routine now to evaluate with modern computer programs the size, the shape and the internal structure (e.g., the hydrophobic core radius and the hydrated hydrophilic shell thickness).
The information about inter-particle interactions in dense systems can be deduced by analyzing the structure factor with various potential models assuming repulsive or attractive interactions. These are considered[44], [53] to play a vital role in the stability of functionalized systems, the residence time or the activity of medicines in the human body, and similar applications.

➤ 6.2. Functionalization of self-assembled structures

Self-assembled structures[42] - [44] have provoked considerable interest in the context of, both, natural and synthetic materials, as they can lead to functional materials with nano-scale structures. The most fundamental tasks in nano-science are

1. the development of nanostructures and

2. understanding (or tuning) their function-property relationship in successful applications.

Small-angle X-ray scattering is taking the leading role in the determination of key relationships between nanostructures and their functions.

6.2.1 Personal health care (cosmetics, toiletry and sanitary)

1. Self-assemblies of amphiphilic molecules, called micelles, are often utilized to solubilize water-insoluble functional substances, such as vitamins, perfumes and many more, in water-based products. Lyotropic liquid crystals in lamellar and reversed hexagonal phases are used for emulsion-type products to improve their stability and viscoelastic properties. The sol-gel structures of amphiphilic molecules, especially their high viscosity and good ability to sustain a considerable amount of water, are widely applied to the productions of shampoos, hair conditioners, and cosmetic creams. In addition, high performance cosmetics are on the market that give a gradual release of ingredients on the skin surface. Liposomes or vesicles consisting of phospholipids or synthetic surfactant bilayers play an essential role and act as nanocapsules.

2. Polymer gels are soft materials that swell due to incorporation of huge amounts of solvent in their three dimensional network of polymer chains. They are widely utilized in sanitary products, baby's diapers, contact lenses, moisturizing agents for dry grounds, etc. Future uses as drug carriers, gel-based actuators, and artificial muscles are also extensively investigated. For instance, a polymer gel consisting of N-isopropyl acryl amide (NIPA) and sodium acrylate possesses hydrophilic and hydrophobic domains in its polymer network. The domain size can be controlled by temperature and/or the adsorption of metal ions and it can be detected by scattering methods. This gives valuable status information about the process of adsorbing materials, for instance, in the recovery of rare or precious metal ions.

3. Inorganic substances also have emerged and play an important role in these fields. For instance, the recent increase in the risk

of skin cancer demands the use of anti-UV foundation creams (sunscreens) against sunburns. These foundations are functionalized by micron to nanometer-sized inorganic (titanium dioxide) particles. However, to avoid damages of the skin caused by the catalytic effects of TiO_2, the particles have to be coated by silica layers with thicknesses in the order of a few nanometers. Specificially engineered inorganic composite particles can, for the first time, act as hypoallergenic functionalized material to protect human skin.

6.2.2 Pharmaceutical materials

For years, much attention has been paid to drug delivery systems that transport drugs directly to the affected parts of the patient's body. A typical and serious example is that anticancer drugs ward off cancer cells but also damage normal cells simultaneously, which causes a number of side effects and lower the patients' quality of life. Drug delivery systems are made of nano-carriers (in the typical size range of 20 to 100 nm) and they shall make it possible to provide the required amount of drugs timely to a specifically affected part with pinpoint accuracy. A wide variety of self-assembly systems (micelles, microemulsions, liposomes, cubosomes, and polymer-gel nano-particles) has been tested as drug carriers. Especially, poly(oxyethylene)-polyamino acid block copolymer stabilized cubosomes of monoglycerides are spotlighted as possible candidates. It is also known that surface-conjugation techniques for drug carriers improve their functions, possibly due to modified inter-particle interactions. Not only nano-assemblies but recombinant and purified proteins with special additives have been earnestly examined as artificial oxygen carriers.

6.2.3 Food and nutrients

The structural information has become more and more important for developing better textures and functionalities that make food products wholesome. Surfactants such as poly(oxyethylene)

sorbitan ester (tween or polysorbate), sucrose ester, and lecithin are added as an emulsifier or solubilizer to many processed food products, forming micelles or liquid crystals. Polymer gels are very appreciated materials in food such as jelly, Japanese-favorite Konnyaku (Konjak), and Tofu (bean curd). They are soft and swelling materials that take up huge amounts of solvent into their three dimensional networks of polymer chains. Nano-structures of triglyceride solids are quite important to obtain good textured chocolate, ice cream, whipped cream, and many more.

6.2.4 Nano-structured inorganic materials

Nano-sized inorganic particles are used in a wide variety of industrial fields such as cosmetics, paints and ceramics production. Among them, mesoporous materials are recently paid much attention to, because of their potential applications as high performance catalysts or molecular sieves. These materials are obtained via ordered nano-templating by surfactant self-assemblies. It is known that chlorophyll extracted from plants is easily damaged by light, but it can be preserved for a long time, if trapped in the (2 - 50 nm) pores of mesoporous silica. Nanostructures matter are anticipated to open the door for the development of solar cells that are more efficient than the conventional silicone-based cells.

➤ 6.3. Nanocomposites

The idea of combining the properties of inorganic nano-colloids with polymers has led to a new class of materials, the so-called nanocomposites. These materials have been described as the next great frontier in material science. They have attracted substantial attention, because of their various industrial applications and because of their academic interest. Particular attention has been given to plate-like particles, such as clays, because of their high aspect ratio (large radius r, small thickness h). Because of this anisotropic structure, nanoclay particles enhance the performance properties of the material, even when small amounts of < 5

wt% are added. An important property of disperse clay particles is their exfoliation into single silicate layers with a thickness of about 1 nm. In order to facilitate the interaction of silicate layers with the polymer, the hydrophilic nature of the clay particles needs to be changed to organophilic. Traditionally, this is achieved by exchanging the metal cations on the exfoliated clay surface by cationic surfactants.

Inorganic nanoparticles (e.g. soot, silica particles, coated silicates, etc.) are used as fillers to enhance the performance of polymeric materials. One aims to improve the thermo-mechanical properties as well as to achieve value-added performance, such as electrical conductivity, thermal conductivity and selective permeability. The characterization of the morphology of the nanoparticles and their degree of dispersion is an important point in developing such nanocomposites. Presently, organically coated silicates are of great interest for the modification of polymeric materials. The morphological behavior of layered silicates, the structure relationship to the desired properties and the quanitification are desirable information to understand and to tune up these materials.

➤ 6.4. Biological nanocomposites

Biological materials, such as shell, bone and tooth are organic-inorganic hybrid composites of protein and mineral with superior strength, hardness and fracture toughness. It is quite remarkable that nature produces such tough materials out of protein constituents as soft as human skin and mineral constituents as brittle as a classroom chalk. Understanding the mechanisms by which nature designs strong and tough composites with weak materials can give us a guideline for the synthesis of man made novel materials. Previous research showed that although they have various hierarchical structures, the biological materials have similar elementary building blocks. X-ray scattering (SAXS) has shown that many biomaterials share a nanostructure consisting of staggered nanoscale mineral structures with very large aspect ratios embedded in a soft protein matrix.

➤ 6.5. Liquid crystals

Condensed matter, which exhibits intermediate thermodynamic phases between the crystalline solid and simple liquid states is called liquid crystal or mesophase. The liquid-crystalline state[45] generally possesses orientational or weak positional order and thus reveals several physical properties of crystals and of liquids. If transitions between the phases are given by temperature, they are called thermotropic. In blends (containing also other components) phase transitions may also depend on concentration, and these liquid crystals are called lyotropic. While thermotropics are at present mostly used for technical applications, lytropics are important for biological systems, e.g. membranes.

Liquid crystals have two main phases, which are called the “nematic phase” and the “smectic phase.” The nematic phase is the simplest of liquid-crystal phases and is close to the liquid phase. The molecules float around as in a liquid phase, but are still ordered in their orientation. The smectic phase is close to the solid phase. The liquid crystals are ordered in layers. Inside these layers, the liquid crystals normally float around freely, but they cannot move freely between the layers.

Since their discovery considerable work has gone into trying to understand the properties of liquid crystals and how these relate to molecular structure. Despite of this work there exists only a poor understanding of how changes in the molecular structure affect the material properties. The SAXS method provides structural information about heterogeneities, aggregate ordering, size, shape, separation and intermolecular spacing within the aggregate stack. It is also useful to study interdependence of morphology and phase behaviour.

The potential applications of liquid crystals are in display technology, optical imaging and recording, light modulators, thermal sensors and biological membranes (drug delivery carriers).

➤ 6.6. Bio-compatible polymers

The name “bio-compatible polymers” has evolved in conjunction with the continuing development of materials used in medical devices. Until recently, a biocompatible material was essentially thought of as one that would “do no harm”. The operative principle was that of inertness, as reflected, for example, in the definition of biocompatibility as “the quality of not having toxic or injurious effects” on biological systems. The discovery of novel polymeric biomaterials - and the refinement of traditional ones - is creating a thoroughly unprecedented excitement in the field as polymer chemists and other materials designers increasingly confront many of the fundamental challenges of medical science. As the biomaterials discipline itself evolves, the startling advances of the last few years in genomics and proteomics, in various high-throughput cell-processing techniques, in supramolecular and permutational chemistry, and in information technology and bioinformatics promise to support the quest for new materials. The tremendous range of current biomaterials research is proposing innovative new polymers for applications ranging from cardiovascular devices to gene therapy. Several of the more interesting formulations are highlighted below.

6.6.1 Protein-based polymers

A series of recently introduced casein-based and soy-based biodegradable thermoplastics have recently joined collagen as a source of natural protein-based biomaterials.
In contrast to collagen, however, these polymers are less susceptible to thermal degradation, can be easily processed via melt-based technologies, and can be reinforced with inert or bioactive ceramics. Temporary replacement implants, scaffolds for tissue engineering, and drug-delivery vehicles are among the potential biomaterials uses under investigation.

6.6.2 Polymers for gene therapy

Concerns about the potential risks associated with viral gene-delivery systems have led to the development of both degradable and nondegradable, targeted and nontargeted polymeric gene carriers. Examples are PLL-PEG-lactose as a carrier for the transfection of plasmid DNA at hepatocytes; a biodegradable cationic polymer, poly(a-[4-aminobutyl]-L-glycolic acid), as a carrier for mouse plasmid DNA to prevent insulitis; and biodegradable gelatin-alginate microspheres as a carrier of adenovirus (Ad5-p53) for intracranial delivery.

6.6.3 Silicon-urethane copolymers

A novel family of silicone-urethane copolymers has been developed that, compared with traditional polyurethane biomaterials, offer advantages in biostability, thromboresistance, abrasion resistance, thermal stability, and surface lubricity, among other properties. Copolymer synthesis is performed via two methods: incorporation of silicone into the polymer backbone together with organic soft segments, and the use of surface-modifying end groups to terminate the copolymer chains. The organic soft block can be either polytetramethyleneoxide (PTMO) or an aliphatic polycarbonate used together with polydimethylsiloxane (PSX). Applications for the new materials include balloons, ventricular assist devices, vascular grafts, pacemaker leads, and orthopedic and urologic implants.

➤ 6.7. Mesoporous materials

These materials have pores that can be periodic, non-periodic or amorphous. Porous materials are classified into three classes, based on their pore diameters d[46]:

microporous ($d < 2$ nm),
mesoporous ($2 \text{ nm} < d < 50$ nm) and
macroporous ($d > 50$ nm).

A narrow pore-size distribution (PSD) gives rise to interesting and important size and shape-dependent properties, such as separation, adsorption and catalysis. Mesoporous materials have pore apertures similar in size to small biological molecules, supramolecules, metal clusters and organometallic compounds. Mesoporous materials that have a narrow pore size distribution may thus be useful as host, support, catalyst and a separation medium for these molecules. Their pore-size distribution critically depends on the method used to synthesize them.

In general, three approaches are used to synthesize inorganic mesoporous materials:

1. propping layered material with pillars
2. aggregating small precursors to form gels and
3. templating inorganic species around organic groups.

In the first approach, organic or inorganic pillars are intercalated into an inorganic host. The pillars prop the layers and create pores. The diffusion of pillars into the host leads to a broad distribution of pillars – the pillar's distance. This anisotropy leads to non-periodic structures with broad pore-size distributions.
In the second approach, small silica species and inorganic polymers are allowed to aggregate and eventually to gelate. This process generally leads to amorphous materials that have broad pore-size distributions. The diffusion paths through the pore system are quite complex.
In the last approach, small inorganic building units are assembled around organic templates to form ordered structures that have narrow pore-size distributions. By using an ensemble of organic molecules to create a larger template, this method can be extended to the synthesis of ordered mesoporous materials.

The original method for making porous materials was to make layered systems supported by pillaring. A guest molecule was introduced into the material and later removed leaving pores. Pillars are used to prevent these pores from collapsing. The sizes of the

pillars decide the size of the pores. With this method it is difficult to get a uniform pore size.

The principle of making materials with a uniform pore size is based on liquid crystal templating. Materials with pore diameters from 2 to 50 nm can be prepared by this method. A three dimensional liquid mixture consisting of long chain surfactants and silica oligomers are used. Micelles, which form spontaneously, are used as templates. As the system gelates, the amorphous silica is cross-linked at just below the boiling point. When the mixture is solid the organic parts are taken away, e.g. by calcination, leaving back open pores.

To determine mesoporous materials properties, such as pore size and distributions, inter-spacing between the pores, surface-to-volume ratios, internal structures, monitoring of aggregation and transformation processes, the SAXS method can be used effectively and in-situ. Metal-doped mesoporous structures for catalytic applications can also be studied concerning the doping effects on structure and distribution.
Therefore, SAXS may generally help to understand and quantify a variety of processes including the synthesis of zeolites and ordered mesoporous silicas (MCM41, SBA15) and their structure-property relationship.

➤ 6.8. Membranes

Biological membranes and their functionality (e.g., as small chemical reactors) strongly depend on the geometrical and chemical properties of the amphiphilic molecules that make up the membrane walls. Membrane parameters such as electron density profile or the flexibility are important parameters to know, because the functionality of the membrane depends on them. For example, the permeability or the tendency to reorganize into micelles, lamellar stacks or vesicles strongly depends on the internal arrangement of the molecules in the bilayers. The inner structure of the

membranes can be modified by pharmaceuticals or by changing the temperature. Drug delivery or gene-transfection strategies can therefore be founded on investigations of the membrane structure. The phospholipid-bilayer membranes such as POPC, DOPC and DPPC can be studied with the SAXS method to obtain their electron density, thickness, repeat distance of lamellae and stacks, number of layers, packing and flexibility parameters.

Polyelectrolyte membrane based fuel cells are a very active area of research. The most significant barrier against running such a fuel cell at elevated temperatures is to maintain the proton conductivity of the membrane. The polyelectrolyte membrane's ability to operate above 120 °C could have benefits for, both, enhanced carbon monoxide (CO) tolerance and improved heat removal. It is required to keep a given amount of water in the membrane. Higher temperature increases the water-vapor pressure, which increases the likelihood that water loss will occur and, thus, significantly reduce the proton conductivity.
The conductivity of a dry membrane is several orders of magnitude lower than a fully saturated membrane. A number of alternative strategies have been investigated to maintain membrane conductivity in a dehydrating environment (i.e. elevated temperature and reduced relative humidity). The addition of an inorganic material into a polymer membrane can alter and improve physical and chemical polymer properties of interest (such as elastic modulus, proton conductivity, solvent permeation rate, tensile strength, hydrophilicity and glass transition temperature) while retaining its important polymer properties to enable operation in the fuel cell. The hydration properties of membranes are key characteristics that can influence fuel-cell performance.

The SAXS method is very useful in studying composite membranes and to establish structure-property relationships.

➤ 6.9. Proteins

6.9.1 Proteins in solution

Proteins are the structures of life, control most of the events of life and their functions are mainly determined by their 3-D structures. Thus, many diseases are linked to the structure state called protein misfolding. Many proteins show vigorous changes in different solution conditions, with the most extreme structure change being protein denaturation. Similar structure changes may happen as a function of time, pH, ionic strength and changes in various solution conditions.

The main purpose of structural molecular biology includes identifying structural states and changes of biological macromolecules and correlating these changes to their biological functions. Over the past decades, 3-D structures of a vast number of biological molecules have been determined[47] using X-ray crystallography and nuclear-magnetic resonance (NMR).
However, these high resolution methods have their own limitations and therefore can be applied only when rather specific conditions are met. For example, a structure determination by X-ray crystallography requires high-quality protein crystals which are complex and costly to produce and their preparation set alone is one of the major disadvantages. NMR overrides this requirement and allows structures in solution to be studied, but the size of the protein typically accessible by NMR is still much smaller than that of X-ray crystallography.
The recent advancements in the development of X-ray scattering instruments allow simultaneous measurements of small and wide-angle X-ray scattering (SWAXS) from proteins in solution. Usually SAXS is used to determine the ternary and quarternary structures by investigating the overall size and shape. SAXS has achieved considerable success in restoring 3-D structures of proteins from the scattering patterns.

However, the limited information in the relatively small q region (<3 nm^{-1}) is an obstacle to the capability to restore 3-D structures.

Therefore, the measurement of X-ray scattering patterns for a variety of proteins should be extended to higher q regions with high accuracy. Experimental set-ups with simultaneous and continous q-range measurements directly probe distance correlations on length scales that are small compared to the overall protein dimensions and may contain rich information of fine-structure details of proteins in solution[48]-[51]. Scattering data in the higher q region is sensitive to protein conformation states (secondary structures and their packing), and also enables scattering patterns to be compared quantitatively with calculated patterns from detailed structure models.
SAXS data can be used as an additional information input for the evaluation of NMR data as well[52], [53].
If time-resolved SWAXS solution has many advantages over time-resolved X-ray crystallography. Firstly, it does not require highly diffracting crystals and this would widen its applicability to more samples. Secondly, any desired conditions, including near physiological ones, can be easily realized. Third, irreversible reactions, which are hard to study with the current time-resolved crystallography, can be studied since a simple flow cell could provide a fresh sample for each physical perturbation.

6.9.2 Protein crystallization

To understand and predict protein crystallization from solutions have been paramount tasks for years. This was motivated by following reasons.

Sufficiently large single crystals are essential to obtain biochemical structure data of proteins using X-ray crystallography. These data are required for drug design and disease treatment.

1. The growth of protein crystals from solution is important in separation and purification of protein products.

2. Protein aggregation takes place in several diseases, such as cataract and sickle-cell anemia.

3. A slow dissolution rate of protein crystals with a narrow size distribution has advantages in drug delivery.

4. The morphology and the quality of crystals keep protein crystallization an active field of research.

A large number of solution parameters take part in the decision for a crystal to grow.[54] Crystallization is a process involving nucleation and growth in general. Crystallization is determined to a large extent by the effective interaction between the molecules and the kinetic factors that control the nucleation and growth. The driving force for crystallization is supersaturation, i.e., the concentration of solute in the solution above the equilibrium solubility. Lowering the temperature, increasing the ionic strength, adjusting the pH and increasing the protein concentration favour the development of supersaturation. In addition, the purity of the protein and the precipitant salt determine the kinetics of crystallization.
The SAXS method is very sensitive in detecting aggregate structures at an early stage and can therefore indicate the optimum conditions for the onset of protein crystallization.

➤ 6.10. Lipoproteins

Many dangerous diseases are associated with changes in the concentration of blood lipoproteins (LPs). Monitoring the risk of heart disease is not as simple as just measuring the cholesterol level.[55] No matter how much cholesterol is carried by the lipoprotein particles, it is the number of various lipoprotein particles that are present that contributes to heart disease. As lipoprotein particles move through the blood, they can enter the wall of an artery. As the

number of lipoprotein particles increases in the blood, more particles move into the walls of arteries. Once inside the artery wall, lipoprotein particles undergo changes that lead to the formation of blockages inside the artery wall. These blockages grow over time leading to increased risk of heart attack. That is why lipoproteins are so important. It is the number of lipoprotein particles that causes heart disease.

Lipoprotein-fractions analysis[56], [57] is particularly important for people with certain risk factors, even if they have normal cholesterol values (LDL cholesterol < 130 mg/dL). A lipoprotein-profile test is most important for people who suffer from heart disease, diabetes and metabolic disorders. But also people, who are exposed to risk factors, such as smoking, high blood pressure, inherited heart diseases and those, who are on cholesterol-lowering medications, will appreciate a lipoprotein-profile test.

SAXS offers fast and precise measurements of LP-particles using only small amounts of sample. Its capability to measure all fractions of lipoproteins simultaneously forms it a cost effective and convenient method for lipoprotein analysis in scientific studies and medical practices.

➤ 6.11. Cancer cells

Breast cancer is a very frequent form of cancer and the leading cause of cancer deaths of women. The lifetime risk of a woman developing breast cancer is as high as 10–13% in the industrial world. Although significant efforts are being made to achieve early detection and effective treatment, yet 20% of all women with breast cancer will die from the disease. Currently diagnosis is based on the so-called triple assessment — a combination of physical examination, mammography using X-rays and/or ultrasound, and fine needle aspiration cytology or core-biopsy.

The histo-pathological assessment relies on alterations to cellular morphology and tissue architecture. Although triple assessment is

effective in detecting most malignant lesions, its sub-optimal specificity means that in some cases open biopsy surgery is required to exclude malignancy. There is therefore a considerable interest in developing diagnostic tools that are specific for the presence of malignant breast tissue.

Each tissue in the breast has its own small-angle scattering (SAXS) pattern, which is directly related to the molecular structure.[58], [59] In particular, SAXS is an excellent tool for studying the supramolecular arrangement of the collagen fibrils. Collagen is the main component of the connective tissue. It is present in the tumoural masses of the breast. Formation of collagen (fibrosis) accompanies the development of breast tumours, either benign or malignant. The supramolecular arrangement of collagen fibrils degrades upon cancer invasion, and it can be revealed by SAXS. Scattering characterisation of the tissues and their pathologies is therefore possible. A SAXS pattern not only carries information about the composition of the sample, but also about the pathology of the tissues. In other words, it can help to determine whether cancer cells have invaded the tissue. Therefore, this method has the potential of being developed as a diagnostic tool.

➤ 6.12. Carbohydrates

Carbohydrates (such as starch) are biologically produced materials which are of enormous economic and industrial importance. As a naturally abundant nutrient carbohydrates are found mainly in the seeds, fruits, tubers, roots, and stem piths of plants, notably in corn, potatoes, wheat, and rice. It's varying widely in appearance according to the source but is commonly prepared as a white amorphous powder.
Carbohydrates consist of two main polysaccharides, amylose and amylopectin. Amylose is essentially linear, whereas amylopectin is highly branched. The structure of native carbohydrate is now thought to be hierarchically organized on four length scales.
1. The molecular scale (<1 nm).
2. The lamellar structure (1 - 10 nm).

3. The growth rings (about 100 nm).
4. The whole granule morphology (about 1000 nm).

Starch is known to adopt a semi-crystalline lamellar structure which consists of stacks of alternating crystalline and amorphous lamellae. The stacks are separated by regions of a second distinct amorphous phase. This non-lamellar amorphous region corresponds to the amorphous growth ring within the starch granule.

Many commercial products have been developed empirically over many years. The structures of these new products stretch from the molecular to the macroscopic length scale and have a substantial impact on the properties of these products. Thus, the knowledge of the structure of native starch and its changes during processing is very desirable.

The structure of starch changes in many processes such as hydrolysis, gelatinization, dissolving, melting, freezing, extrusion and many more. For example, the staling of bread is mainly the result from the transformation (i.e., retrogradation) of the starch during aging. Also many other compounds such as gluten, water soluble proteins and lipids play a important role in bread staling.

The SAXS method is very useful in investigating[60], [61] both, native starch and starch products. For native starch, the SAXS method allows the study of structure and changes in the structure, lamellar repeat distance, fractional lamellar crystallinity, width of the distribution of lamellar sizes, the number of semi-crystalline repeats within each growth ring whose details characterize the starch structure. For starch products, the SAXS method is used rarely, as a result from the fact that the lamellae of amyloptectin are quite collapsed or seriously destroyed. Starch is not the only component in these materials, which makes the analysis of SAXS data more complex than in native pure starch. However, for this kind of starch materials (food products) the SAXS method also allows many values to be obtained which can undoubtedly be useful in classifying the properties of these material.

➤ 6.13. Building materials

The study of the kinetics and mechanism of hydration of cement materials is of prime importance for achieving desirable mechanical properties of the hardened products, and to control the reactivity of the raw mixtures (the starting material). The main phases in a typical Portland cement can be subdivided into calcium silicates as the main component and calcium aluminates as the minor component. During the hydration of an anhydrous cement, the chemical reactions are generally more complex than simple conversions of anhydrous compounds into the corresponding hydrates. Hydrated cement has a high specific surface almost entirely due to the calcium-silicate-hydrate (C-S-H) reaction product. It is closely related to many properties including strength and permeability.
It is also useful to study the nature of the C-S-H gel itself. The microstructure of cement is quite complex. It contains several reacted products, unreacted clinker grains and voids, which are responsible for the porosity. One major challenge in the measurement of the surface in hydrating cement paste arises from the involved heterogeneous microstructure and the applicable large range of length scales (from few nanometers to tens of micrometers).

When using SAXS, one of the advantages is that they can be conducted in real time during cement hydration without interfering the hydration process. This has allowed the development of a method[62], [63] to monitor the C-S-H gel structure and the surface area from the earliest stage of a few minutes. Instruments with a large q-range, a high resolution with calibrated absolute-intensity data and scattering contrast method is preferable to obtain the surface area. The advantage of a surface area measurement is significant, because it is sensitive to the C-S-H gel phase which controls to some extent every property in cement-based materials. This makes the surface-area parameter useful, both, for the investigation of the C-S-H-gel structure, and for relating the effects of processing and composition to the final properties of cement paste and concrete.

➤ 6.14. Minerals

Particles of fine-grained minerals are everywhere in terrestrial, marine and atmospheric environments. They are a major constituent of soils, they form colloidal suspensions in oceans and terrestrial water bodies and are a major component of atmospheric aerosols. Their abundance, high surface area, reactivity and colloidal characteristics mean that they play an important role within many processes occurring in the natural environment including chemical weathering, bio-mineralisation, transport pollutants in ground waters and the global cycle of elements. The nano-particulate nature of these mineral phases means that their chemistry (e.g., their solubility) and phase stability are different from bulk phases of the same composition. The implications for the natural environment require investigations on the nanoscale.
The nucleation and growth of mineral particles is often associated with hydrolysis reactions which, at first sight, are the simplest reactions of metal ions, but nevertheless play a fundamental role in industrial chemistry (e.g., production of pigments, magnetic media), effluent treatment (aluminum flocs in drinking water treatment, iron flocs in the removal of radioactive and toxic metals) and environmental and atmospheric processes (e.g., aerosol formation). Particle shape/size and growth rate, in particular, are fundamental controls on the properties of the hydrolysis reaction products and SAXS is the only technique which can provide this information,[64] when the particles are suspended in solution. It is however still a challenge, when investigations have to be made on fast timescales associated with particle formation.

➤ 6.15. GI-SAXS applications

Basically all of the above mentioned applications of ordinary transmission-mode SAXS can be applied to investigate the material properties in thin films. The difference is that with the combination of GI-SAXS, XRR and “constant-q scanning” the thin-film structures can be investigated in all three dimensions. This is also

necessary, because the molecules of the thin-film materials align themselves epitactically with the substrate, adsorb to it or react with the substrate.

The interaction of thin-film materials with substrate materials can be investigated specifically. For example, block copolymers undergo microphase separation and the two domains have different adhesion-properties towards the surface. Therefore, the domains orient themselves and parallel or perpendicular versions of the microdomain phases will result. These cases can be readily distinguished with GI-SAXS.
These phase-separated thin-films can undergo additional structure changes when treated with the vapors of solvents[65] or when thermal treatment (e.g. annealing)[66] is applied. The softening of one or all microdomains can lead to higher degrees of order.

Once the self-assembly structures are brought onto the substrate surface, they can be used as a template to deposit functional oxide materials in a second coating. Calcination then leads to a structured coating of functional oxides, the success of which can be followed with GI-SAXS.[67]

Instead of block copolymers also colloidal particles, such as latex spheres,[68], [69] discotic liquid crystals[70] or pigment particles of varnishes and paints can be investigated as well. Adhesive films develop their properties in surface-near regions. Structures that develop parallel to the surface were detected with GI-SAXS and are thought to be responsible for the adhesion quality.[71]

Metal surfaces tend to react with the surrounding environment producing coatings made of reaction products. The formation of these layers leads to homogeneous coatings or to simple corrosion spots (islands) which can be distinguished by checking the surface roughness.

Biomaterials, i.e., materials that are compatible with biological tissues are frequently tested by checking the adhesion properties of

globular proteins on their surface. GI-SAXS can help to prove the formation of protein coatings.

It goes without saying that coatings of surfactants,[72] lipids[73] and biocompatible polymers on flat substrates can also be characterized with GI-SAXS in terms of homogeneity of deposition, orientation, self-assembly structures and interaction properties with peptides.

➤ 6.16. Conclusion

During the last decade, small-angle X-ray scattering has become an increasingly important tool in studying the diverse fields of material science. This process has been accelerated by the accessibility of large-scales facilities and the availability of latest high-performance laboratory instruments along with the availability of novel and powerful data-analysis programs. Judging from the momentum that was gained in the last decade by using SAXS and the technique's inherent and unique capability in addressing the steadily up-coming developments in nanomaterials suggests that, in future, SAXS will further strengthen its position as a mainstream method for the analysis in a multiplicity of fields in material-science research.

7. Literature

[1] A. Guinier and G. Fournet, Small-Angle Scattering of X-rays (Wiley, New York, 1955).

[2] O. Glatter and O. Kratky (edts.), Small-Angle X-ray Scattering (Academic, London, 1982).

[3] O. Glatter and R. May, "2.6. Small-angle techniques ," in A.J.C. Wilson and E. Prince (edts.), International Tables for Crystallography C (Kluwer Academic Publishers, Dordrecht, 1999).

[4] C. Giacovazzo,"The diffraction of X-rays by crystals" in C. Giacovazzo, H. L. Monaco, D. Viterbo, F. Scordari, G. Gilli, G. Zanotti and M. Catti (edts.), Fundamentals of crystallography (IUCr Texts on Crystallography No. 2.) (Oxford University, Oxford, 1992).

[5] J.S. Higgins and H.C. Benoît, Polymers and Neutron Scattering (Clarendon, Oxford, 1994).

[6] M. Kerker, The Scattering of Light and Other Electromagnetic Radiation (Academic, New York, 1969).

[7] D.C. Creagh and J.H. Hubbell, "X-ray absorption (or attenuation) coefficients," in A.J.C. Wilson (edt.), International Tables for Crystallography, Vol. C, Sec. 4.2.4., 189-206 (Kluwer Academic, Dordrecht, 1992).

[8] J.H. Hubbell, Wm.J. Veigele, E.A. Briggs, R.T. Brown, D.T. Cromer and R.J. Howerton, "Atomic form factors, incoherent scattering functions, and photon scattering cross sections," J. Phys. Chem. Ref. Data **4**, 471-538 (1975); erratum in **6**, 615-616 (1977).

[9] J.H. Hubbell and I. Øverbø, "Relativistic atomic form factors and photon coherent scattering cross sections," J. Phys. Chem. Ref. Data 8, 69-105 (1979).

[10] D.T. Cromer and J.T. Waber, “Atomic Scattering Factors for X-Rays,” in International Tables for X-Ray Crystallography, Vol. 4, Sec. 2.2., 71-147 (Kynoch Press, Birmingham, 1974).

[11] G. Goerigk, H.G. Haubold, O. Lyon and J.P. Simon, “Anomalous small-angle X-ray scattering in materials science,” J. Appl. Cryst. **36**, 425-429 (2003).

[12] L.G. Parratt, “Surface studies of solids by total reflection of X-rays,” Phys. Rev. **95**, 359-369 (1954).

[13] A. Gibaud and S. Hazra, “X-ray reflectivity and diffuse scattering,” Current Science **78**, 1467-1477 (2000).

[14] M. Tolan, X-Ray Scattering from Soft-Matter Thin Films (Springer Tracts in Modern Physics, Volume 148, Berlin, 1999).

[15] S.K. Sinha, E.B. Sirota, S. Garoff and H.B. Stanley, “X-Ray and neutron scattering from rough surfaces,” Phys. Rev. B **38**, 2297-2311 (1988).

[16] W. Weber and B. Lengeler, “Diffuse scattering of hard x rays from rough surfaces,” Phys. Rev. B **46**, 7953-7956 (1992).

[17] V. Holy, J. Kubena, I. Ohlidal, K. Lischka and W. Plotz, “X-Ray reflection from rough layered systems,” Phys. Rev. B **47**, 15896-15903 (1993).

[18] V. Holy and T. Baumbach, “Non-specular x-ray reflection from rough multilayers,” Phys. Rev. B **49**, 10668-10676 (1994).

[19] R. Lazzari, “IsGISAXS: a program for grazing-incidence small-angle X-ray scattering analysis from supported islands,” J. Appl. Cryst. **35**, 406-421 (2002).

[20] J.A. Lake, “An iterative method of slit-correcting small angle X-ray data,” Acta Cryst. **23**, 191-194 (1967).

[21] G.R. Strobl, “A new method for evaluating slit-smeared small angle X-ray scattering data,” Acta Cryst. **A26**, 367-375 (1970).

[22] O. Glatter, “A new method for the evaluation of small-angle scattering data,” J. Appl. Cryst. **10**, 415-421 (1977).

[23] R.N. Bracewell, The Fourier Transform and Its Applications, (McGraw-Hill, New York, 1965).

[24] I. Pilz, chapter 8, page 248 in O. Glatter and O. Kratky (edts.), Small-Angle X-ray Scattering (Academic, London, 1982).

[25] D. Orthaber, A. Bergmann and O. Glatter, “SAXS experiments on absolute scale with Kratky systems using water as a secondary standard,“ J. Appl. Cryst. **33**, 218-225 (2000).

[26] H. Stabinger and O. Kratky, “A new technique for the measurement of absolute intensity of X-ray small angle scattering. The moving slit method,” Makromol. Chem. **179**, 1655-1659 (1978).

[27] G. Fritz, A. Bergmann, and O. Glatter, “Evaluation of small-angle scattering data of charged particles using the generalized indirect Fourier transformation technique,” J. Chem. Phys. **113**, 9733-9740 (2000).

[28] R. Mittelbach and O. Glatter, “Direct structural analysis of small-angle scattering data from polydisperse colloidal particles,” J. Appl. Cryst. **31**, 600-608 (1998).

[29] G. Fritz and A. Bergmann, “Interpretation of small-angle scattering data of inhomogeneous ellipsoids,” J. Appl. Cryst. **37**, 815-822 (2004).

[30] O. Glatter, “Computation of distance distribution functions and scattering functions of models for small angle scattering experiments,” Acta Phys. Austriaca **52**, 243-256 (1980).

[31] D. Svergun, C. Barberato, M.H.J. Koch, "CRYSOL – a program to evaluate X-ray solution scattering of biological macromolecules from atomic coordinates," J. Appl. Cryst. **28**, 768-773 (1995).

[32] P. Chacon, F. Moran, J.F. Diaz, E. Pantos, J.M. Andreu, "Low-resolution structures of proteins in solution retrieved from X-ray scattering with a genetic algorithm," Biophys. J. **74**, 2760-2775 (1998).

[33] P. Chacon, J. F. Diaz, F. Moran, and J. M. Andreu, "Reconstruction of protein form with X-ray solution scattering and a genetic algorithm," J. Mol. Biol. **299**, 1289-1302 (2000).

[34] D. Svergun "Restoring low resolution structure of biological macromole-cules from solution scattering using simulated annealing," Biophys. J. **76**, 2879-2886 (1999), erratum in **77**, 2896-2896 (1999).

[35] D.K. Cinader and W.R. Burghardt, "X-ray scattering studies of orientation in channel flows of a thermotropic liquid–crystalline polymer," J. Polym. Sci.,Part B: Polym.Phys. **37**, 3411-3428 (1999).

[36] S. Steenstrup, "A simple procedure for fitting a backgound to a certain class of measured spectra," J. Appl. Cryst. **14**, 226-229 (1981).

[37] S. Kim, G. Jin, M. Lim, "Structural dynamics of myoglobin probed by femtosecond infrared spectroscopy of the amide band," Bull. Korean Chem. Soc. **24**, 1470-1474 (2003).

[38] M. Wulff, A. Plech, L. Eybert, R. Randler, F. Schotte, P. Anfinrud, "The realization of sub-nanosecond pump and probe experiments at the ESRF," Faraday Discussions **122**, 13-26 (2003).

[39] F. Schotte, M.H. Lim, T.A. Jackson, A.V. Smirnov, J. Soman, J.S. Olson, G.N. Phillips, M. Wulff, P.A. Anfinrud, "Watching a protein as it functions with 150-ps time-resolved X-ray crystallography," Science **300**, 1944-1947 (2003).

[40] S. Techert, F. Schotte, M. Wulff, "Picosecond X-ray diffraction probed transient structural changes in organic solids," Phys. Rev. Lett. **86**, 2030-2033 (2001).

[41] S. Bratos, F. Mirloup, R. Vuilleumier, M. Wulff, "Time-resolved X-ray diffraction: Statistical theory and its application to the photo-physics of molecular iodine," J. Chem. Phys. **116**, 10615-10625 (2002).

[42] G.M. Whitesides, J.P. Mathias, C.T. Seto, "Molecular self-assembly and nanochemistry: A chemical strategy for the synthesis of nanostructures," Science **254**, 1312-1319 (1991).

[43] G.M. Whitesides, B. Crzybowski, "Self-assembly at all stages," Science **295**, 2418-2421 (2002).

[44] M. Muthukumar, C.K. Ober, E.L. Thomas, "Competing interactions and levels of ordering in self-organizing polymeric materials," Science **277**, 1225-1232 (1997).

[45] P.J. Collings, Liquid Crystals (Adam Hilger, Bristol, 1990).

[46] K. S. W. Sing, D. H. Everett, R. A. W. Haul, L. Moscou, R. A. Pierotti, J. Rouquerol, T. Siemieniewska, Pure Appl Chem 57, 603–619 (1985).

[47] A.M. Edwards, C.H. Arrowsmith, D. Christendat, A. Dharamsi, J.D. Friesen, J.F. Greenblatt, M. Vedadi, "Protein production: feeding the crystallographers and NMR spectroscopists," Nat. Struct. Biol. **7**, 970-972 (2000).

[48] R.F. Fischetti, D.J. Rodi, A. Mirza, T.C. Irving, E. Kondrashkina, L. Makowski, "High-resolution wide-angle X-ray scattering of protein solutions: Effect of beam dose on protein integrity," J. Synchrotron Rad. **10**, 398-404 (2003).

[49] M. Hirai, H. Iwase, T. Hayakawa, K. Miura, K. Inoue, "Structural hierarchy of several proteins observed by wide-angle solution scattering," J. Synchrotron Rad. **9**, 202-205 (2002).

[50] D.M. Tiede, R. Zhang, S. Seifert, "Protein conformations explored by difference high-angle solution X-ray scattering: Oxidation state and temperature dependent changes in cytochrome c," Biochemistry **41**, 6605-6614 (2002).

[51] R. Zhang, P. Thiyagarajan, D.M. Tiede, "Probing protein fine structures by wide angle solution X-ray scattering," J. Appl. Cryst. **33**, 565-568 (2000).

[52] D.I. Svergun and M.H.J. Koch, "Small-angle scattering studies of biological macromolecules in solution," Rep. Prog. Phys. **66**, 1735–1782 (2003).

[53] J. Trewhella and J.K. Krueger, "Small-angle solution scattering reveals information on conformational dynamics in calcium-binding proteins and in their interactions with regulatory targets," Methods Mol. Biol. **173**, 137–159 (2002).

[54] J. Narayanan and X.Y. Liu, "Protein interactions in undersaturated and supersaturated solutions: A study using light and X-ray scattering," Biophys. J. **84**, 523-532 (2003)

[55] H.B. Brewer Jr., R.E. Gregg, J.M. Hoeg, "Apolipoproteins, lipoproteins, and atherosclerosis," in E. Braunwald (edt.) Heart Disease: A Textbook of Cardiovascular Medicine, p.121-144 (WB Saunders, New York, 1989).

[56] Y.P. Nikitin, F.V. Tuzikov, N.A. Tuzikova, Y. Ragino, "Application of the small-angle X-ray scattering technique for estimation structural change of lipoprotein fractions of blood," Abstracts of 71st European Atherosclerosis Society **73**, 26-29 (1999).

[57] F.V. Tuzikov, L.E. Panin, N.A. Tuzikova, L.M. Poljakov, "Application of the small-angle X-ray scattering technique for estimating structural changes at high density lipoproteins," Membr. Cell Biol. **10**, 75-82 (1996).

[58] R.A. Lewis, K.D. Rogers, C.J. Hall, E. Towns-Andrews, S. Slawson, A. Evans, S.E. Pinder, I.O. Ellis, C.R.M. Boggis, A.P. Hufton and D.R. Dance, "Breast cancer diagnosis using scattered X-rays," J. Synchrotron Rad. **7**, 348–352 (2000).

[59] M. Fernández, J. Keyriläinen, R. Serimaa, M. Torkkeli, M-L. Karjalainen-Lindsberg, M. Tenhunen, W. Thomlinson, V. Urban and P. Suortti, "Small-angle X-ray scattering studies of human breast tissue samples," Phys. Med. Biol. **47**, 577-592 (2002).

[60] S. Pikus, "Small-angle X-ray scattering (SAXS) studies of the structure of starch and starch products," Fibres and Textiles in Eastern Europe **13**, 82-86 (2005).

[61] P.A. Perry, T.A. Waigh, A.M. Donald, "The effect of changing solvents on the kinetics and micromechanics of starch freezing," Annual Report of the Synchrotron Radiation Department of the CLRC Daresbury Laboratory, p.110-111 (1997-1998).

[62] J.J. Thomas, H.M. Jennings and A.J. Allen, "The surface area of cement paste as measured by neutron scattering - Evidence for two C-S-H morphologies," Cement and Concrete Research **28**, 897–905 (1998).

[63] J.J. Thomas, H.M. Jennings and A.J. Allen, "The surface area of hardened cement paste as measured by various techniques," Concrete Science and Engineering **1**, 45-64 (1999).

[64] S. Shaw, L.G. Benning, N.J. Terrill, C.M.B. Henderson and J.A. Warner, "In Situ SAXS/WAXS Studies of the Precipitation, Crystallization and High Temperature Phase Transitions of Minerals," 30th Annual report of the Stanford Synchrotron Radiation Laboratory, (2003).

[65] C.M. Papadakis, Z. Di, D. Posselt and D-M. Smilgies, "Structural instabilities in lamellar diblock copolymer thin films during solvent vapor uptake," Langmuir **24**, 13815-13818 (2008).

[66] A. Sepe, E.T. Hoppe, S.Jaksch, D.Magerl, Q.Zhong, J.Perlich, D.Posselt, D-M.Smilgies and C.M.Papadakis, "The effect of heat treatment on the internal structure of nanostructured block copolymer films," J. Phys.: Condens. Matter **23**, 254213-254215 (2011).

[67] Z. Sun, M. Wolkenhauer, G.G. Bumbu, D.H. Kim, J.S. Gutmann, "GISAXS investigation of TiO2 nanoparticles in PS-b-PEO block-copolymer films," Physica B **357**, 141-143 (2005).

[68] S. Park, D.H. Lee, J. Xu, B. Kim, S.W. Hong, U. Jeong, T. Xu and T.P. Russell, "Macroscopic 10-Terabit-per-Square-Inch Arrays from Block Copolymers with Lateral Order," Science **323**, 1030-1033 (2009).

[69] S. Hu, J. Rieger, S.V. Roth, R. Gehrke, R.J. Leyrer and Y. Men, "GIUSAXS and AFM studies on surface reconstruction of latex thin films during thermal treatment", Langmuir **25**, 4230-4234 (2009).

[70] H.S. Kim, S.M. Choi, J.H. Lee, P. Busch, S.J. Koza, E.A. Verploegen, B.D. Pate, "Uniaxially Oriented, Highly Ordered, Large Area Columnar Superstructures of Discotic Supramolecules using Magnetic Field and Surface Interactions," Adv. Mater. **20**, 1105–1109 (2008).

[71] A.Diethert, K.Ecker, Y.Peykova, N.Willenbacher and P. Müller-Buschbaum, “Tailoring the near-surface composition profiles of pressure sensitive adhesive films and the resulting mechanical properties,” ACS Appl. Mater. Interfaces **3**, 2012-2021 (2011).

[72] P. Siffalovic, E. Majkova, L. Chitu, M. Jergel, S. Luby, A. Satka, and S. V. Roth, “Self-assembly of iron oxide nanoparticles studied by time-resolved grazing-incidence small-angle x-ray scattering,” Phys. Rev. B **76**, 195432-195439 (2007).

[73] T. Salditt, C. Li and A. Spaar, “Structure of antimicrobial peptides and lipid membranes probed by interface-sensitive X-ray scattering,” Biochimica et Biophysica Acta 1758, 1483–1498 (2006).

8. Index

ISBN 18012013

9 783900 323882

Anton Paar

Anton Paar® GmbH
Anton-Paar-Str. 20, A-8054 Graz
Austria - Europe
Tel.: +43 (0)316 257-0
Fax: +43 (0)316 257-257
E-mail: info@anton-paar.com
Web: www.anton-paar.com